Simulations of the redistribution of formaldehyde, formic acid, and peroxides in the 10 July 1996 Stratospheric-Tropospheric Experiment: Radiation, Aerosols, and Ozone deep convection storm

M. C. Barth,[1] S.-W. Kim,[1,2] W. C. Skamarock,[1] A. L. Stuart,[3] K. E. Pickering,[4,5] and L. E. Ott[4,6]

Received 15 September 2006; revised 15 March 2007; accepted 16 April 2007; published 12 July 2007.

[1] By using a three-dimensional convective cloud model to simulate the 10 July 1996, Stratospheric-Tropospheric Experiment: Radiation, Aerosols, and Ozone-Deep Convection experiment storm, we investigate the fate of formaldehyde (CH_2O), formic acid (HCOOH), hydrogen peroxide (H_2O_2), and methyl hydrogen peroxide (CH_3OOH) in an isolated thunderstorm. CH_2O, H_2O_2, and CH_3OOH are important HO_x radical and ozone (O_3) precursors in the upper troposphere. Thus, determining their source strength to the upper troposphere is important for estimating O_3 production. The model simulates O_3-NO_x-CH_4 chemistry (no nonmethane hydrocarbon chemistry) which is affected by the cloud microphysics and production of NO_x by lightning. The retention of the soluble species within ice, snow, and hail during drop freezing results in less transport of the species to the upper troposphere than when the species is degassed during drop-freezing processes. Aqueous-phase chemistry is found to be inadequate in producing sufficient quantities of HCOOH so that HCOOH could serve as a reliable indicator of cloud-processed air. The production of nitrogen oxides by lightning has little to no effect on convective outflow mixing ratios of CH_2O, H_2O_2, and CH_3OOH within 100 km of the convective cores. Thus, it is unlikely that lightning affects concentrations of HO_x precursors near active convection. Scavenging of CH_2O and H_2O_2 significantly affects their concentrations in the convective outflow, although H_2O_2 mixing ratios were still similar to CH_3OOH indicating that both peroxides can contribute equally to O_3 production downwind of convection.

Citation: Barth, M. C., S.-W. Kim, W. C. Skamarock, A. L. Stuart, K. E. Pickering, and L. E. Ott (2007), Simulations of the redistribution of formaldehyde, formic acid, and peroxides in the 10 July 1996 Stratospheric-Tropospheric Experiment: Radiation, Aerosols, and Ozone deep convection storm, *J. Geophys. Res.*, *112*, D13310, doi:10.1029/2006JD008046.

1. Introduction

[2] Deep convection plays an important role in redistributing chemical constituents. Convective transport rapidly moves chemical constituents from the boundary layer to the upper troposphere (UT) resulting in a C-shaped vertical profile [e.g., *Chatfield and Crutzen*, 1984; *Dickerson et al.*, 1987]. Once in the upper troposphere, the chemical species generally have a longer lifetime and therefore are more likely to be transported globally. Chemical consequences of the transport of boundary layer air to the upper troposphere can be to increase ozone (O_3) to mixing ratios greater than those in the undisturbed atmosphere [*Pickering et al.*, 1992b]. Ozone in the UT impacts the Earth's radiation budget, the UV flux to the surface, and the production of radical species that are responsible for removal of primary pollutants. Thus, quantifying the influx of ozone and its precursors to the UT via deep convection improves our understanding of the ozone budget in the upper troposphere.

[3] Ozone production depends on the relative amounts of its precursors, the nitrogen oxides nitric oxide (NO) and nitrogen dioxide (NO_2), which together are known as NO_x, and the hydrogen oxides hydroxyl radical (OH) and hydroperoxy radical (HO_2) which together are known as HO_x. Thunderstorms provide an abundance of NO_x to the upper

[1]National Center for Atmospheric Research, Boulder, Colorado, USA.
[2]Now at National Oceanic and Atmospheric Administration, Earth Systems Research Laboratory and Cooperative Institute for Research in Environmental Studies, University of Colorado, Boulder, Colorado, USA.
[3]Department of Environmental and Occupational Health, University of South Florida, Tampa, Florida, USA.
[4]Department of Atmospheric and Oceanic Science, University of Maryland, College Park, Maryland, USA.
[5]Now at Laboratory for Atmospheres, NASA Goddard Space Flight Center, Greenbelt, Maryland, USA.
[6]Now at Global Modeling and Assimilation Office, NASA Goddard Space Flight Center, Greenbelt, Maryland, USA.

0148-0227/07/2006JD008046

troposphere via NO production from lightning [*Ridley et al.*, 1996]. Once in the UT, the longer NO_x lifetimes and the relatively more dilute concentrations result in a higher potential for producing ozone [*Liu et al.*, 1987; *Pickering et al.*, 1990] compared to the boundary layer.

[4] HO_x precursors, such as hydrogen peroxide (H_2O_2), methyl hydrogen peroxide (CH_3OOH), and formaldehyde (CH_2O), are also important to ozone production rates [*Chatfield and Crutzen*, 1984; *Prather and Jacob*, 1997; *Jaeglé et al.*, 1997; *Wennberg et al.*, 1998; *Jaeglé et al.*, 2001]. These species are by-products of photochemistry and thus have their greatest mixing ratios in the boundary layer relatively near emission sources. Transport by deep convection redistributes these species so that there may be an increase in concentration in the upper tropospheric convective outflow. However, H_2O_2 and CH_2O are soluble species such that a fraction of the species is scavenged by the storm and removed by wet deposition. H_2O_2 and CH_2O are also reactive species in the aqueous phase and their concentrations can be reduced by reaction of H_2O_2 with aqueous sulfur dioxide or by oxidation of CH_2O to form formic acid (HCOOH). The fate of these soluble species is sensitive to the cloud microphysics. *Barth et al.* [2001] found when snow or hail collects cloud or raindrops, retention of a soluble tracer in a frozen particle during cloud drop freezing removed the species from the upper troposphere while degassing the soluble tracer during cloud drop freezing allowed for tracer transport to the UT. Cloud scattering of solar radiation, which alters the photodissociation rates, and adsorption of the gas-phase species onto ice can also affect the mixing ratios of H_2O_2, CH_3OOH, and CH_2O [*Wang and Prinn*, 2000; *Wang*, 2005]. As a result of these processes, the flux of HO_x precursors to the upper troposphere is less certain because these species are subject to multiple processes in the deep convection.

[5] The goal of this paper is to examine the redistribution of formaldehyde and peroxides in a midlatitude, continental thunderstorm, and to estimate their scavenging efficiencies and fluxes to the upper troposphere. The sensitivity of these quantities to different convective processes (for example, chemistry, microphysics, and lightning-produced NO) is discussed. This study is done using the Weather Research and Forecasting (WRF) model coupled with a simple gas and aqueous chemistry module (WRF-AqChem). The model is configured to perform an idealized simulation of convection representing the 10 July 1996, Stratospheric-Tropospheric Experiment: Radiation, Aerosols, and Ozone-Deep Convection (STERAO) experiment which was conducted in northeastern Colorado.

[6] Previous studies have examined the redistribution of passive tracers (for example, CO and O_3) by deep convection [e.g., *Pickering et al.*, 1992a; *Scala et al.*, 1990; *Hauf et al.*, 1995]. These previous studies examined storms occurring in different environmental conditions and with different degrees of entrainment. As a result, the tracer transport characteristics (for example, inflow region, tracer amount in the outflow) varied in these studies. There are several previous studies of sulfur dioxide (SO_2) transport and scavenging in convective clouds [e.g., *Flossmann and Wobrock*, 1996; *Tremblay*, 1987; *Wang and Crutzen*, 1995; *Mari et al.*, 2000; *Yin et al.*, 2002]. In general, it was found that there was only a small amount of SO_2 transported to the free troposphere primarily because in-cloud oxidation destroyed SO_2.

[7] More recently, *Wang and Prinn* [2000] examined the effects of deep convection on tropospheric chemistry for a tropical, oceanic storm (observed during CEPEX on 8 March 1993) using a convective-scale cloud chemistry model. They found that the HO_x precursors, CH_2O and H_2O_2, both increased in the upper troposphere because of deep convection. Wang and Prinn determined that these increased UT mixing ratios originated from a layer residing just above the boundary layer and avoided significant removal into cloud drops because this source layer was ingested into the storm above the freezing level. *Wang and Prinn* [2000] also found an increase of CH_2O due to higher NO mixing ratios from lightning production which increased the rate of the $CH_3OO + NO$ gas-phase reaction.

[8] *DeCaria et al.* [2005] used a chemistry transport model driven by the Goddard Cumulus Ensemble (GCE) model to simulate the 12 July 1996 STERAO storm. Their results show increases of HO_x, H_2O_2, CH_3OOH, and CH_2O in the upper troposphere as a result of vertical transport. Wet scavenging of these species is performed in all model grid cells containing liquid water. Because their chemistry model is run offline of the meteorology model, *DeCaria et al.* [2005] were not able to investigate effects of the microphysics on these soluble, reactive species because of freezing of water droplets or transformations from one hydrometeor category to another.

2. Model Description

[9] The WRF model is the host meteorological model. The model solves the conservative (flux-form), nonhydrostatic compressible equations [*Skamarock et al.*, 2005] using a split-explicit time-integration method based on a third-order Runge-Kutta scheme [*Wicker and Skamarock*, 2002]. Scalar transport is integrated with the Runge-Kutta scheme using fifth-order (horizontal) and third-order (vertical) upwind-biased advection operators. Transported scalars include water vapor, cloud water, rain, cloud ice, snow, graupel (or hail), and chemical species. The WRF dynamics and transport exactly conserves mass and scalar mass to machine round off. While mass is conserved, the scheme is not positive definite. However, results from other WRF simulations show that moisture added by this scheme is only 2–5% of the total condensate. The ice microphysics parameterization is that described by *Lin et al.* [1983]. For the simulations performed here, hail hydrometeor characteristics (ρ_h = 917 kg m^{-3}, No = 4 $\times$ 104 m^{-4}) are used.

[10] The model predicts the mixing ratios of 16 chemical species (Table 1). The gas-phase chemistry (Table 2) represents daytime chemistry of 15 chemical species. The chemical mechanism represents the chemistry of ozone, nitrogen oxides, carbon monoxide, and methane but does not include nonmethane hydrocarbon chemistry. The lack of NMHC chemistry can significantly affect HO_x precursors, such as CH_2O, and therefore HO_x concentrations in the upper troposphere [*Jaeglé et al.*, 2001]. Rate coefficients are from the work of *Sander et al.* [2003]. The diurnally varying, gas-phase photolysis rates are results for clear-sky calculations using the Tropospheric Ultraviolet and Visible radiation model [*Madronich and Flocke*, 1999] for 10 July at 41°N

Table 1. Accommodation Coefficients Into Water for Each of the Species

Species	Accommodation Coefficient
O_3	0.00053
H_2O_2	0.02
OH	0.05
HO_2	0.20
CH_3OO	0.05
CH_3OOH	0.05
CH_2O	0.05
HCOOH	0.05
NO	0.005
NO_2	0.00063
HNO_3	0.05
NH_3	0.05
SO_2	0.05
SO_4^{2-}	0.05
CO	–
CH_4	–

and for an overhead ozone column of 290 Dobson units. The beginning of the model simulation was set to 1600 local time. The aqueous chemistry (Table 3), whose rates are from the works of *Lelieveld and Crutzen* [1991] and *Hoffmann and Calvert* [1985], is computed for the cloud water and rain in which the pH is iteratively calculated via a charge balance assuming CO_2 is 360 ppmv. The Henry's law equilibrium constants (Table 4), which are from the work of *Sander* [1999], are used to determine the partitioning between gas and aqueous phases. For gas-liquid interactions, the accommodation coefficients (Table 1) follow *Lelieveld and Crutzen* [1991]. The chemical mechanism is solved with an Euler backward iterative approximation using a Gauss-Seidel method with variable iterations. A convergence criterion of 0.01% is used for all the species.

[11] The interaction between the gas phase and the condensed phase for the chemical species is a critical aspect that is examined in this study. Transport of species between the gas phase and the liquid hydrometeors is assumed to be

Table 2. Gas Phase Reactions

		k_{298} [a]	$-\frac{E}{R}$
(G1)	$O_3 + h\nu \rightarrow 2\ OH$	4.93×10^{-5} [b]	0.0
(G2)	$HO_2 + O_3 \rightarrow OH + 2O_2$	2.0×10^{-15}	500.0
(G3)	$OH + O_3 \rightarrow HO_2 + O_2$	6.8×10^{-14}	940.0
(G4)	$HO_2 + OH \rightarrow H_2O + O_2$	1.1×10^{-10}	−250.0
(G5)	$OH + OH + O_2 \rightarrow O_3 + H_2O$	1.9×10^{-12}	240.0
(G6)	$OH + OH + M \rightarrow H_2O_2 + M$	$k_o = 6.9 \times 10^{-31}\left(\frac{T}{300}\right)^{-0.8}$	
		$k_\infty = 1.5 \times 10^{-11}$	
(G7)	$HO_2 + HO_2 \rightarrow H_2O_2 + O_2$	$k_a = 1.7 \times 10^{-12}$ [c]	−600.0
		$k_b = 4.9 \times 10^{-32}$	−1000.0
		$k_c = 2.24 \times 10^{-18}$	−2200.0
(G8)	$H_2O_2 + h\nu \rightarrow 2\ OH$	1.23×10^{-5}	0.0
(G9)	$H_2O_2 + OH \rightarrow HO_2 + H_2O$	1.7×10^{-12}	160.0
(G10)	$NO + O_3 \rightarrow NO_2 + O_2$	1.8×10^{-14}	1400.0
(G11)	$HO_2 + NO \rightarrow OH + NO_2$	8.6×10^{-12}	−250.0
(G12)	$NO_2 + h\nu \rightarrow NO + O_3$	1.1×10^{-2}	0.0
(G13)	$OH + NO_2 + M \rightarrow HNO_3 + M$	$k_o = 2.6 \times 10^{-30}\left(\frac{T}{300}\right)^{-3.2}$	
		$k_\infty = 2.4 \times 10^{-11}\left(\frac{T}{300}\right)^{-1.3}$	
(G14)	$HNO_3 + h\nu \rightarrow OH + NO_2$	9.89×10^{-7}	0.0
(G15)	$HNO_3 + OH \rightarrow 0.89\ NO_2 + 0.89\ O_3 + 0.11\ NO$	$k_a = 1.0 \times 10^{-13}$ [d]	−785.
		$k_b = 2.16 \times 10^{-32}$	−725.0
		$k_c = 5.13 \times 10^{-14}$	−1440.0
(G16)	$CH_4 + OH + O_2 \rightarrow CH_3OO + H_2O$	6.3×10^{-15}	1800.0
(G17)	$CH_3OO + NO + O_2 \rightarrow CH_2O + NO_2 + HO_2$	7.7×10^{-12}	−180.0
(G18)	$CH_3OO + HO_2 \rightarrow CH_3OOH + O_2$	5.6×10^{-12}	−800.0
(G19)	$CH_3OO + HO_2 \rightarrow CH_2O + H_2O + O_2$	2.0×10^{-12}	0.0
(G20)	$CH_3OO + CH3OO + O_2 \rightarrow 1.4\ CH_2O + 0.8\ HO_2 + 0.6$ R(O)OH[e]	4.7×10^{-13}	−190.0
(G21)	$CH_3OOH + h\nu + O_2 \rightarrow CH_2O + OH + HO_2$	1.15×10^{-5}	0.0
(G22)	$CH_3OOH + OH \rightarrow .7\ CH_3OO + .3\ CH_2O + .3\ OH$	7.4×10^{-12}	−200.0
(G23)	$CH_2O + h\nu + 2\ O_2 \rightarrow CO + 2\ HO_2$	4.95×10^{-5}	0.0
(G24)	$CH_2O + h\nu \rightarrow CO + 2\ H_2$	6.93×10^{-5}	0.0
(G25)	$CH_2O + OH + O_2 \rightarrow CO + HO_2 + H_2O$	1.0×10^{-11}	0.0
(G26)	$CO + OH + O_2 \rightarrow CO_2 + HO_2$	2.4×10^{-13} [f]	0.0
(G27)	$HCOOH + OH + O_2 \rightarrow CO_2 + HO_2 + H_2O$	3.2×10^{-13}	0.0
(G28)	$SO_2 + OH + M \rightarrow SO_4^{2-} + HO_2 + M$	$k_o = 3.0 \times 10^{-31}(\frac{T}{300})^{-3.3}$	0.0
		$k_\infty = 1.5 \times 10^{-12}$	

[a] Units for the photolysis frequencies are s^{-1}, for the second-order reaction rate constants are cm^3 $molecules^{-1}$ s^{-1}, and for the third-order reaction rate constants are cm^6 $molecules^{-2}$ s^{-1}. Photolysis rate values are noontime values for 10 July at 40°N; the simulation follows a diurnal profile. Second-order reaction rate constants are of the form $k = k_{298}\exp[-\frac{E}{R}\left(\frac{1}{298} - \frac{1}{T}\right)]$. Third-order reaction rate constants are of the form $k = k_o\,[M] / (1. + k)\ 0.6^{\phi}$ where $k = k_o\,[M] / k_\infty$, $\phi = ([1 + \log_{10}(k)]^2)^{-1}$ and $[M]$ is the air concentration. Reaction rate coefficients are from the work of *Sander et al.* [2003].

[b] The O_3 photolysis rate is computed as $j_{O_3} = j_1(2.2 \times 10^{-10}[H_2O] / (2.2 \times 10^{-10}[H_2O] + 2.9 \times 10^{-11}[M]))$ where $[H_2O]$ is the water vapor concentration.

[c] Here, the rate constant is of the form $k = (k_a + k_b\,[M])\ (1 + k_c\,[H_2O])$.

[d] Here, the rate constant is of the form $k = k_a + k_b\,[M] / 1 + k_b\,[M] / k_c$.

[e] R(O) OH is a higher order organic acid that is not predicted by the model.

[f] The CO + OH reaction rate constant has the form 1.5×10^{-13} $(1 + 0.6 \sim P_{atm})$.

Table 3. Aqueous-Phase Reactions

		k_{298} [a]	$-\frac{E}{R}$
(A1)	$O_3 + h\nu + H_2O \rightarrow H_2O_2 + O_2$	–	
(A2)	$H_2O_2 + h\nu \rightarrow 2\ OH$	–	
(A3)	$CH_2(OH)_2 + OH + O_2 \rightarrow HCOOH + HO_2 + H_2O$	2.0×10^9	−1500.
(A4)	$HCOOH + OH + O_2 \rightarrow CO_2 + HO_2 + H_2O$	1.6×10^8	−1500.
(A5)	$HCOO^- + OH + O_2 \rightarrow CO_2 + HO_2 + OH^-$	2.5×10^9	−1500.
(A6)	$CH_3OO + O_2^- + H_2O \rightarrow CH_3OOH + OH^- + O_2$	5.0 × 107	−1600.
(A7)	$CH_3OOH + OH \rightarrow CH_3OO + H_2O$	2.7×10^7	−1700.
(A8)	$CH_3OOH + OH \rightarrow CH_2(OH)_2 + OH$	1.9×10^7	−1900.
(A9)	$HO_2 + O_2^- \rightarrow HO_2^- + O_2$	1.0×10^8	−1500.
(A10)	$O_3 + O_2^- + H_2O \rightarrow OH + 2O_2 + OH^-$	1.5×10^9	−1500.
(A11)	$H_2O_2 + OH \rightarrow HO_2 + H_2O$	2.7×10^7	−1700.
(A12)	$OH + O_2^- \rightarrow OH^- + O_2$	1.0×10^{10}	−1500.
(A13)	$HSO_3^- + H_2O_2 \rightarrow SO_4^{2-} + H_2O + 2H^+$	2.7×10^7 [b]	4750.
(A14)	$HSO_3^- + O_3 \rightarrow SO_4^{2-} + H^+ + O_2$	3.7×10^5	5300.
(A15)	$SO_3^{2-} + O_3 \rightarrow SO_4^{2-} + O_2$	1.5×10^9	5280.

[a]Units for the photolysis frequencies are s^{-1}, and for the second-order reaction rate coefficients are $M^{-1}\ s^{-1}$. Reaction rate coefficients are from the work of *Lelieveld and Crutzen* [1991] and for S(IV) oxidation from the work of *Hoffmann and Calvert* [1985]. Reaction rates coefficients are of the form $k = k_{298}\exp[-\frac{E}{R}(\frac{1}{T}-\frac{1}{298})]$. Photolysis rate constants are 1.5 times greater than their gas phase counterparts.

[b]Here the reaction rate coefficient is of the form $k = k[H^+] / (1 + 13[H^+])$.

in Henry's law equilibrium for many of the species, however, this assumption is checked at each time step and grid cell by comparing the amount of a species in the liquid hydrometeors calculated by Henry's law equilibrium to the liquid-phase amount of the species calculated by diffusion-limited mass transport [*Schwartz*, 1986]. If Henry's law equilibrium cannot be reached in the model time step of 10 s, then diffusion-limited mass transport determines the partitioning between gas and aqueous phases. The partitioning of the species OH, HO_2, CH_3OO, HNO_3, and NH_3 between gas and aqueous phases is always calculated by the diffusion-limited mass transport calculation. More details on this algorithm are given in the work of *Barth et al.* [2001].

[12] Species that are absorbed into the condensed phase can subsequently be moved from one hydrometeor category to another. For example, when rain collects cloud water, the dissolved chemical species is transferred from the cloud water reservoir to the rain reservoir. The calculation is done in the same manner as in the work of *Barth et al.* [2001]. The importance of freezing on dissolved species is examined in a sensitivity simulation. The control simulation assumes that the dissolved chemical species is completely retained in the frozen hydrometeor when cloud or raindrops freeze, while the sensitivity simulation assumes that all of the dissolved species is degassed during freezing. These assumptions bound the problem. When frozen particles (ice, snow, or hail) sublimate, the species is retained in the frozen particle until all of the water mass at the grid point has transferred to the gas phase.

3. Conditions of the Simulations

[13] A description of the meteorological scenario and transport of passive tracers is given by *Skamarock et al.* [2000] for the 10 July 1996 STERAO storm. In the same manner, we initialize the model environment with a single sounding for pressure, potential temperature, and horizontal wind speeds. Three warm bubbles of 3°C perturbation and oriented in the northwest-southeast direction are used to initiate the convection.

[14] The model is configured to a 160 × 160 × 20 km^3 domain with 161 grid points in each horizontal direction (1-km resolution) and 50 grid points in the vertical direction with a variable resolution beginning at 50 m at the surface and stretching to 1000 m at the top of the domain. The vertical grid spacing between 8 and 15 km a.g.l. ranges from 500 m at 8 km to 900 m at 15 km. The simulation is integrated for 3 hours and a time step of 10 s is used.

[15] Most chemical species are initialized (Figure 1) with values measured in the inflow region of the storm; other species are estimated from values found in the literature or

Table 4. Equilibrium Coefficients

		k_{298} [a]	$-\frac{\Delta H}{R}$
(E1)	O_3 (g) ⇌ O_3 (aq)	1.15×10^{-2}	2560.
(E2)	H_2O_2 (g) ⇌ H_2O_2 (aq)	8.33×10^4	7379.
(E3)	OH (g) ⇌ OH (aq)	30.	0.
(E4)	HO_2 (g) ⇌ HO_2 (aq)	$2. \times 10^3$	6600.
(E5)	CH_3OO (g) ⇌ CH_3OO (aq)	7.47	5641.
(E6)	CH_3OOH (g) ⇌ CH_3OOH (aq)	3.11×10^2	5241.
(E7)	CH_2O (g) ⇌ $CH_2(OH)_2$ (aq)	6.3×10^3	6425.
(E8)	HCOOH (g) ⇌ HCOOH (aq)	5.53×10^3	5700.
(E9)	NO (g) ⇌ NO (aq)	1.9×10^{-3}	1480.
(E10)	NO_2 (g) ⇌ NO_2 (aq)	6.4×10^{-3}	2500.
(E11)	HNO_3 (g) ⇌ HNO_3 (aq)	2.1×10^5	8700.
(E12)	CO (g) ⇌ CO (aq)	1.0×10^{-3}	0.
(E13)	CH_4 (g) ⇌ CH_4 (aq)	1.7×10^{-3}	0.
(E14)	NH_3 (g) ⇌ NH_3 (aq)	92.7	4085.
(E15)	SO_2 (g) ⇌ SO_2 (aq)	1.23	3120.
(E16)	SO_4^{2-} (g) ⇌ SO_4^{2-} (aq)	1.0×10^{15}	0.
(E17)	CO_2 (g) ⇌ CO_2 (aq)	3.4×10^{-2}	2200.
	Acid Dissociation Equilibria		
(E18)	H_2O_2 (aq) ⇌ $HO_2^- + H^+$	2.2×10^{-12}	−3700.
(E19)	HO_2 (aq) ⇌ $O_2^- + H^+$	3.5×10^{-5}	0.
(E20)	HCOOH (aq) ⇌ $HCOO^- + H^+$	1.8×10^{-4}	−1500.
(E21)	HNO_3 (aq) ⇌ $NO_3^- + H^+$	15.4	0.
(E22)	SO_2 (aq) ⇌ $HSO_3^- + H^+$	1.3×10^{-2}	2000.
(E23)	HSO_3^- ⇌ $SO_3^{2-} + H^+$	6.3×10^{-8}	1500.
(E24)	NH_3 (aq) ⇌ $NH_4OH + OH^-$	1.7×10^{-5}	−450.
(E25)	CO_2 (aq) ⇌ $HCO_3^- + H^+$	4.5×10^{-7}	−1000.
(E26)	HCO_3^- ⇌ $CO_3^{2-} + H^+$	3.61×10^{-11}	−1760.

[a]Units for solubility constants are $M\ atm^{-1}$, and units for dissociation constants are M. Coefficients are of the form $k = k_{298}\exp[-\frac{\Delta H}{R}(\frac{1}{T}-\frac{1}{298})]$. Equilibrium coefficients are from *Sander* [1999].

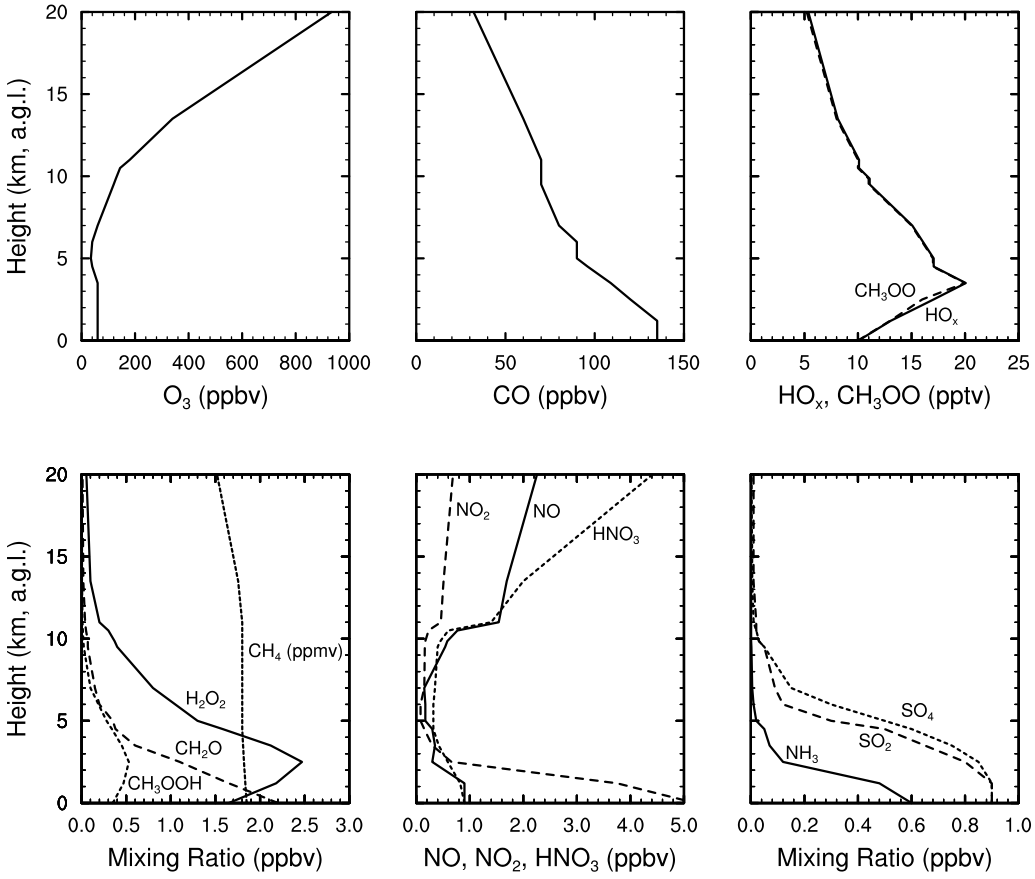

Figure 1. Initial mixing ratios of species included in the simulations. NO and NO_2 mixing ratios are 10 times smaller than shown (i.e., surface NO_2 = 0.5 ppbv). HCOOH initial mixing ratio is 0.

from the July monthly mean mixing ratio for northeastern Colorado calculated by the three-dimensional global transport model, MOZART [*Brasseur et al.*, 1998]. OH, HO_2 and NO, NO_2 quickly come into equilibrium with the HO_x and NO_x families, respectively.

[16] Several simulations (Table 5) are performed to explore the importance of various processes on CH_2O, H_2O_2, and CH_3OOH. The control simulation (pH-Calc) includes both gas and aqueous-phase chemistry, which uses a calculated pH. The pH is diagnosed from a charge balance assuming ammonium sulfate for the CCN and dissolved SO_2, NH_3, HNO_3, HCOOH, HO_2, and CO_2 (whose gas-phase mixing ratio is prescribed to 360 ppmv). When cloud or raindrops freeze, all of the dissolved species are retained in the frozen hydrometeor (ice, snow, or hail). There is no production of NO_x from lightning in the pH-Calc simulation. The pH = 4.5 simulation is the same as the pH-Calc simulation except that the pH is prescribed to 4.5 everywhere. The Degassed simulation is the same as the pH-Calc simulation except that dissolved species are completely degassed when cloud or raindrops freeze.

[17] The L(NOx)-On simulation is the same as the pH-Calc simulation with the additional NO_x source from lightning. The parameterization included for this simulation follows the work of *DeCaria et al.* [2005]. Conceptually, NO_x is produced in a region where reflectivity is >20 dBZ and is distributed vertically following either a Gaussian distribution (cloud-to-ground flash) peaking in the midtroposphere or a bimodal distribution (intracloud flash) with peaks in the upper troposphere and midtroposphere. Observed lightning flash rates calculated from the National Lightning Detection Network (NLDN) and interferometer observations [*Dye et al.*, 2000] are used as input to trigger lightning production of NO_x (termed here as L(NOx)). As in the work of *DeCaria et al.* [2005], only flashes with durations greater than 100 ms are included in the flash rate calculations. A cloud-to-ground flash is assumed to produce on average 390 moles of NO based on the mean peak current observed by the NLDN for this storm and a relationship between peak current and energy dissipated from the work of *Price et al.* [1997]. Through a comparison of in-cloud aircraft observations and model results for this storm, an intracloud flash is estimated to produce 195 moles of NO on average. These estimates of NO production per

Table 5. Simulations Performed

Simulation	Gas Chemistry	Aqueous Chemistry	Retention of Species During Freezing	Production of NO from Lightning
pH-Calc	On	On (pH calc)	Retained	No
pH = 4.5	On	On (pH = 4.5)	Retained	No
Degassed	On	On (pH calc)	Degassed	No
L(NOx)-On	On	On (pH calc)	Retained	Yes
No-AqChem	On	Off	Retained	No
No-Chem	Off	Off	Retained	No

flash are larger than the approximately 43 moles of NO per interferometer flash estimated by *Skamarock et al.* [2003] because that study included a large number of flashes with durations less than 100 ms. Whether or not these short duration flashes produce NO remains an open question. The production per CG flash assumed in this study agrees favorably with the 460 moles of NO per CG flash estimated by *DeCaria et al.* [2005] for the 12 July STERAO storm. In addition, two recent modeling studies [*Fehr et al.*, 2004; *Ott et al.*, 2007] estimated that a CG flash produced 360 and 330 moles of NO, respectively, in a storm observed in Germany.

[18] The No-AqChem simulation is the same as the pH-Calc simulation except that there is no aqueous chemistry occurring in the cloud and raindrops. Chemical species are still partitioned between the gas and aqueous phases so that wet deposition of species occurs. The No-Chem simulation is the same as the pH-Calc simulation except that there is no chemistry occurring at all. As in the No-AqChem simulation, partitioning between gas and aqueous phases still occurs. This simulation indicates the importance of convective transport of a species.

4. Results

4.1. Storm Structure

[19] In order to determine whether the storm simulated by the WRF-AqChem model represents the storm structure that was observed, a comparison of the modeled reflectivity to observed radar reflectivity is performed (Figure 2). We examine two times, one during the multicellular stage of the storm (at 1 hour of model integration) and one during the quasi-supercellular stage of the storm (at 2.5 hours of model integration). The radar reflectivity plots show that the modeled cloud successfully transitions from a multicellular storm to a single cell storm. The radar intensities are similar between model and observations, but the orientation of the modeled storm at t = 2.5 hours is more east-west than the observations. The anvil region produced by the WRF-AqChem model is narrower than the observations. The width of the anvil is most likely determined by the microphysics parameterization. Modeling studies of BAMEX storms using different microphysics parameterizations indicate that schemes that predict only the mass mixing ratio of the cloud particles produce smaller anvil areas, while those that predict both number and mass produce widespread anvils [*Seifert and Weisman*, 2005]. An intercomparison of model results for the 10 July 1996 STERAO storm also shows this trend [*Barth et al.* 2007]. Despite these inconsistencies with the observations, the model results represent the observed storm structure reasonably well.

[20] The primary pathway for chemical species to be scavenged by cloud hydrometeors is via absorption into cloud drops. Thus, the amount and location of the cloud water and the other cloud hydrometeors are critical to the analysis of cloud scavenging. The modeled hydrometeor fields, shown as a vertical cross section through the convective cells in Figure 3, exhibit a narrow region of cloud water, a somewhat larger region of hail, and a broad anvil composed of snow. At t = 1 hour, cloud water mixing ratios reach values >0.5 g kg^{-1}, rain mixing ratios reach values >1.0 g kg^{-1}, snow mixing ratios reach values of >3 g kg^{-1}, and hail mixing ratios are between 0.5 and 1.5 g kg^{-1}. At t = 1.5 hours, cloud water remains in the core of the cell, with mixing ratios reaching 2.5 g kg^{-1}. Rain mixing ratios are generally <1.5 g kg^{-1}. There is an extensive snow anvil in which mixing ratios reach values up to 3.5 g kg^{-1}. Hail, again, is found mostly in the core of the storm, with mixing ratios reaching 7 g kg^{-1}.

4.2. Chemistry

[21] For all the simulations listed in Table 5 the transport of CO and O_3 by the simulated convection is essentially the same because the cloud processes (both chemical and physical) do not strongly affect these relatively insoluble, long-lived species (long-lived compared to the timescale of the convection). Results from the pH-Calc simulation are presented here and results from the other simulations are discussed as sensitivities to the pH-Calc simulation. The redistribution of CO and O_3 is first discussed and evaluated with aircraft observations, which included across anvil measurements that are appropriate to compare to model results during the first 2 hours of simulation. Therefore the following results are discussed at t = 1 hour when the simulated and observed storm is multicellular and t = 1.5 hours when the simulated storm is transitioning to a single cell storm.

[22] Similar to the works of *Skamarock et al.* [2000] and *Barth et al.* [2001], CO is transported from the boundary layer to the anvil (Figure 4) where mixing ratios are >110 ppbv and are much greater than the unperturbed UT at the same level. The convection transports relatively low mixing ratios of O_3 (~60 ppbv) from the boundary layer to the upper troposphere where background mixing ratios are 100–150 ppbv. The perturbation in the anvil region is seen 50 km or so downwind of the southeasternmost convective cell for both t = 3600 s and t = 5400 s during the simulation.

[23] To evaluate the ability of the model to predict transport of passive tracers, modeled CO and O_3 are compared to aircraft observations in the anvil region (Figure 5). These plots illustrate good agreement between modeled results and observations, especially in the center of the anvil. As with the radar reflectivity, the model results show a more narrow outflow region of CO and O_3 than the measurements resulting in an underprediction of CO on the northeast (right-side of plots) section of the observed anvil. Near the southwest (left-side of plots) edge of the anvil, the observed O_3 is higher than the modeled O_3, where mixing of stratospheric air is not being represented by the model likely because of the coarse vertical resolution (Δz = 600 m at z = 10 km).

[24] On the basis of these results, we are confident that the WRF-AqChem model transports passive constituents from the boundary layer to the upper troposphere in a realistic manner. In the next section, we discuss results of soluble and reactive species for which we do not have observations in the anvil. The discussion will focus on comparison of the soluble species to less soluble species and on the sensitivity of the soluble species to processes parameterized in the model.

[25] Results of several species along the two transects (marked as C-D and G-H in Figure 4) are shown (Figure 6) to give an idea of what would be sampled by an aircraft during an across-anvil transect. For soluble species, both

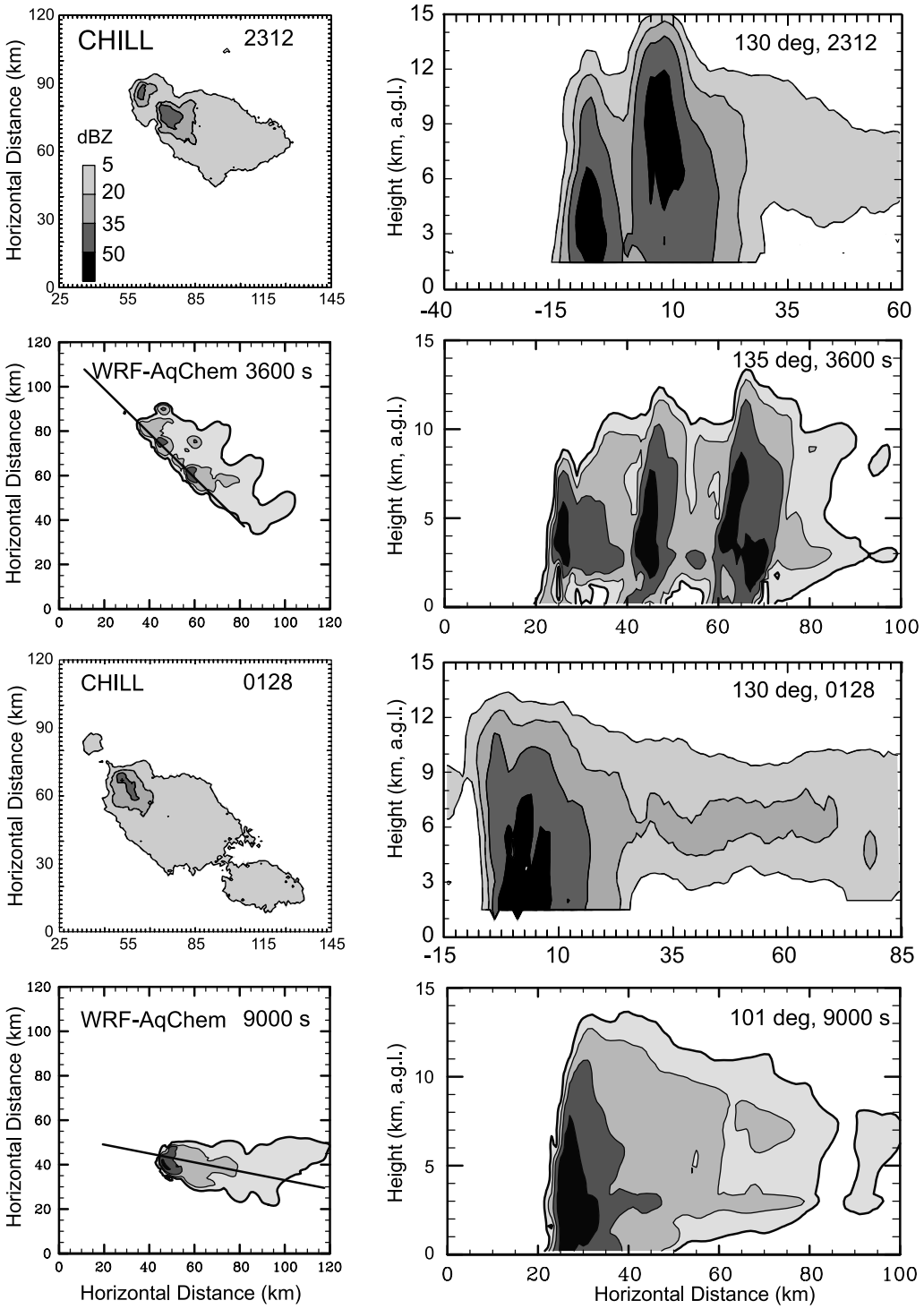

Figure 2. Radar reflectivity from the CSU CHILL radar (first and third rows) and from the model results (second and fourth rows) at 9 km above ground level (first column) and vertical cross section along the storm axis (second column). The first two rows are at 2312 UTC (CHILL radar) and t = 3600 s of model simulation. The second two rows are at 0128 UTC (CHILL radar) and t = 9000 s of model simulation.

gas-phase mixing ratios and total [sum of species mixing ratio in the gas phase, cloud water, rain, ice, snow, and hail, where condensed-phase mixing ratios are also expressed in moles per mole air] mixing ratios are plotted. CH_2O, HNO_3, and H_2O_2 are all depleted in the anvil for both transects (at 10 and 50 km downwind of the storm core) because of scavenging and precipitation. CH_3OOH, SO_2, NO_x, and HCOOH are enhanced in the anvil compared to outside the anvil region. For t = 3600 s and 10 km downwind of the storm core, CH_2O, HCOOH, and H_2O_2 have a significant

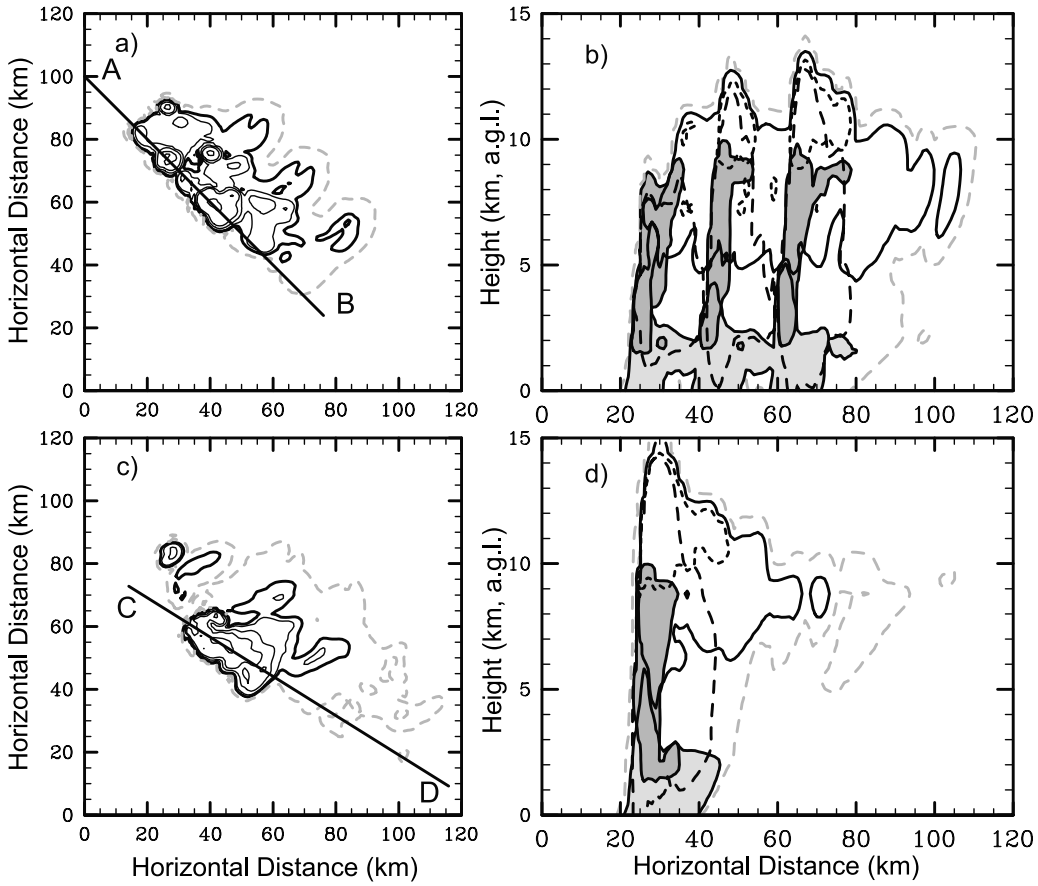

Figure 3. Hydrometeor mixing ratios (g kg^{-1}) from the model simulation for (a) snow at 10 km above ground level (a.g.l.) and t = 3600 s; (b) cloud water (dark-shaded region), rain (light-shaded region), ice (dotted line), snow (solid line), and hail (black dashed line) along the AB cross section at t = 3600 s; (c) snow at 10 km a.g.l. and t = 5400 s; and (d) cloud water (dark-shaded region), rain (light-shaded region), ice (dotted line), snow (solid line), and hail (black dashed line) along the CD cross section at t = 5400 s. The contour level is 0.1 g kg^{-1}. The dashed gray line is the total condensate mixing ratio equal to 0.01 g kg^{-1}.

fraction in the cloud hydrometeors, while at t = 5400 s at 50 km downwind of the storm core, most of the soluble species is in the gas phase where less liquid water exists. The radical species (Figures 6b and 6f) indicate a small depletion within the anvil region at t = 5400 s but have a larger depletion at t = 3600 s and 10 km downwind of the storm core where more liquid condensate resides.

[26] Comparisons of the composition in the anvil to that in the boundary layer allow us to determine if species other than CO and O_3 are conserved and to estimate the degree of entrainment. Transport of CO and O_3 for this same simulated storm in the context of entrainment is also discussed by *Skamarock et al.* [2000]. Relative to CO and O_3 boundary layer mixing ratios of 135 and 60 ppbv, the anvil air with their lower (higher) mixing ratios exhibits moderate entrainment for CO and O_3, respectively. A two-component mixture model [*Cohan et al.*, 1999] would suggest that ~45% of the air is entrained. Using the same methodology for other species such as NO_x is more problematic because of its sharp gradient in the boundary layer. Nevertheless, the NO_x mixing ratios in the convective outflow compared to the boundary layer also shows moderate entrainment. Thus, NO_x is approximately conserved when its source from lightning does not occur. CH_2O, HNO_3, H_2O_2, CH_3OOH, and SO_2 have total mixing ratios in the anvil that are much smaller than what one expects from passive tracer transport with ~45% entrainment indicating that scavenging and chemistry are also depleting the mixing ratios of these species.

4.3. Formaldehyde

[27] Formaldehyde is an important intermediate of methane oxidation. It is produced from methyl peroxy radicals reacting with nitric oxide (G17, Table 2), from the self reaction of methyl peroxy radicals (G20), or from methyl hydrogen peroxide oxidation by OH (G22). Formaldehyde is destroyed either by photodissociation (G23-G24) or by oxidation with OH (G25). In the aqueous phase, formaldehyde is oxidized to form formic acid (A3, Table 3).

[28] Because CH_2O and CO have similar initial vertical profiles, it is useful to compare the redistribution of CH_2O, a soluble, reactive species, to CO, an insoluble, passive (on timescales of convection) species. The horizontal and vertical cross sections of total CH_2O (Figure 7; total CH_2O = sum of CH_2O in all the hydrometeors plus CH_2O in the gas phase) show that much less total CH_2O reaches the UT than

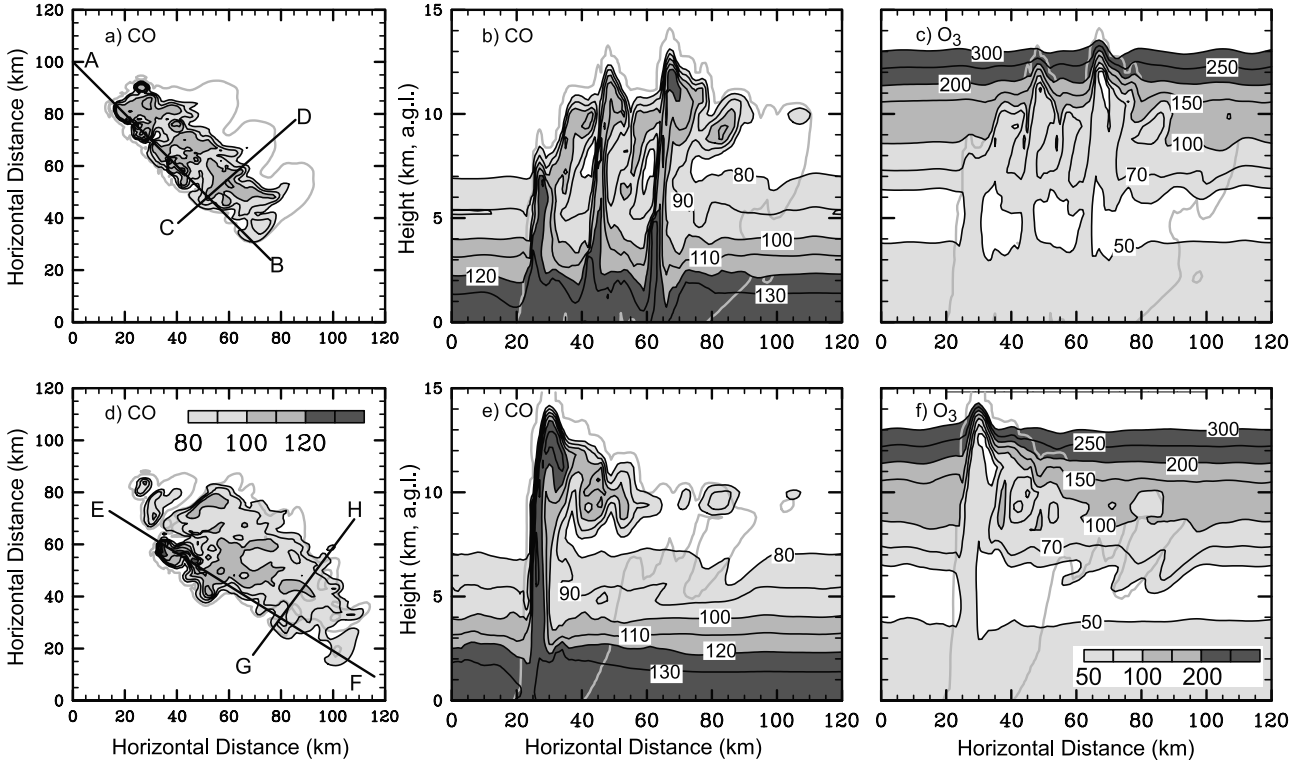

Figure 4. CO and O_3 model results from the pH-Calc (control) simulation at (a–c) t = 3600 s and at (d–f) t = 5400 s. Horizontal cross sections (panels a and d) of CO (ppbv) at 10 km a.g.l. Vertical cross sections along the storm axis (indicated by lines A-B and E-F in the horizontal cross sections) of (b and e) CO (ppbv) and of (c and f) O_3 (ppbv). The gray line is the total condensate mixing ratio equal to 0.01 g kg^{-1}. In Figures 4a and 4d, the C-D and G-H lines refer to the across anvil transects shown in Figure 5.

CO (Figure 4). At 10 km a.g.l., the anvil contains regions of depleted CH_2O compared to the boundary layer and background UT, indicating a fraction of CH_2O has reacted or precipitated to the ground or lower troposphere.

[29] To show the influence of cloud processing on CH_2O, the ratio of CH_2O to CO is examined. The vertical cross section along the storm axis (Figure 8) shows that high ratios of total CH_2O to CO are transported from the boundary layer to the upper troposphere. Uptake of CH_2O in the storm core is seen by the strong depletion of gas-phase CH_2O to CO ratio (Figures 8c and 8f). In the convective outflow region, the ratio is depleted compared to both the background UT and the boundary layer CH_2O to CO ratios. There is greater depletion near the storm core than further downwind where gas-phase CH_2O mixing ratios are larger. Note that the ratios for the unperturbed troposphere shown in Figure 8 are somewhat smaller than what would be found from measurements. Boundary layer

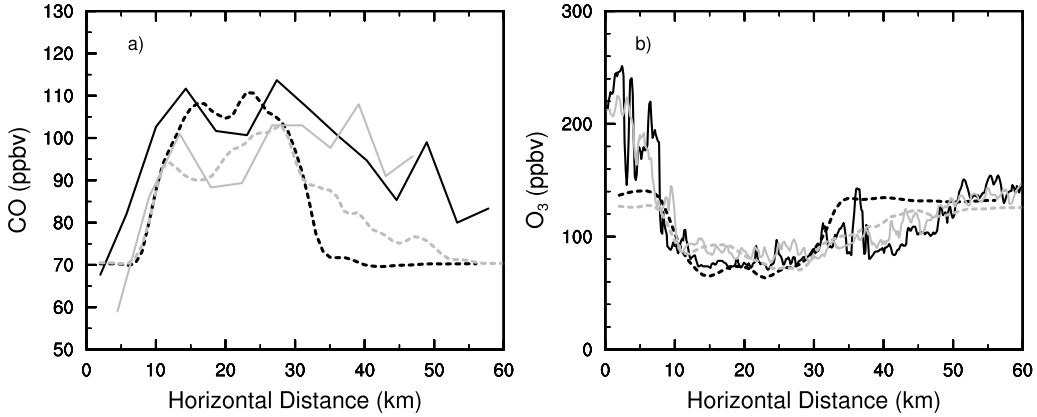

Figure 5. (a) CO and (b) O_3 measurements (solid lines) from the UND Citation aircraft for anvil passes 10 km (z = 10.1 km a.g.l., black lines) and 50 km (z = 9.7 km a.g.l., gray lines) downwind of the southeasternmost cell. Dashed lines are model results from the pH-Calc (control) simulation.

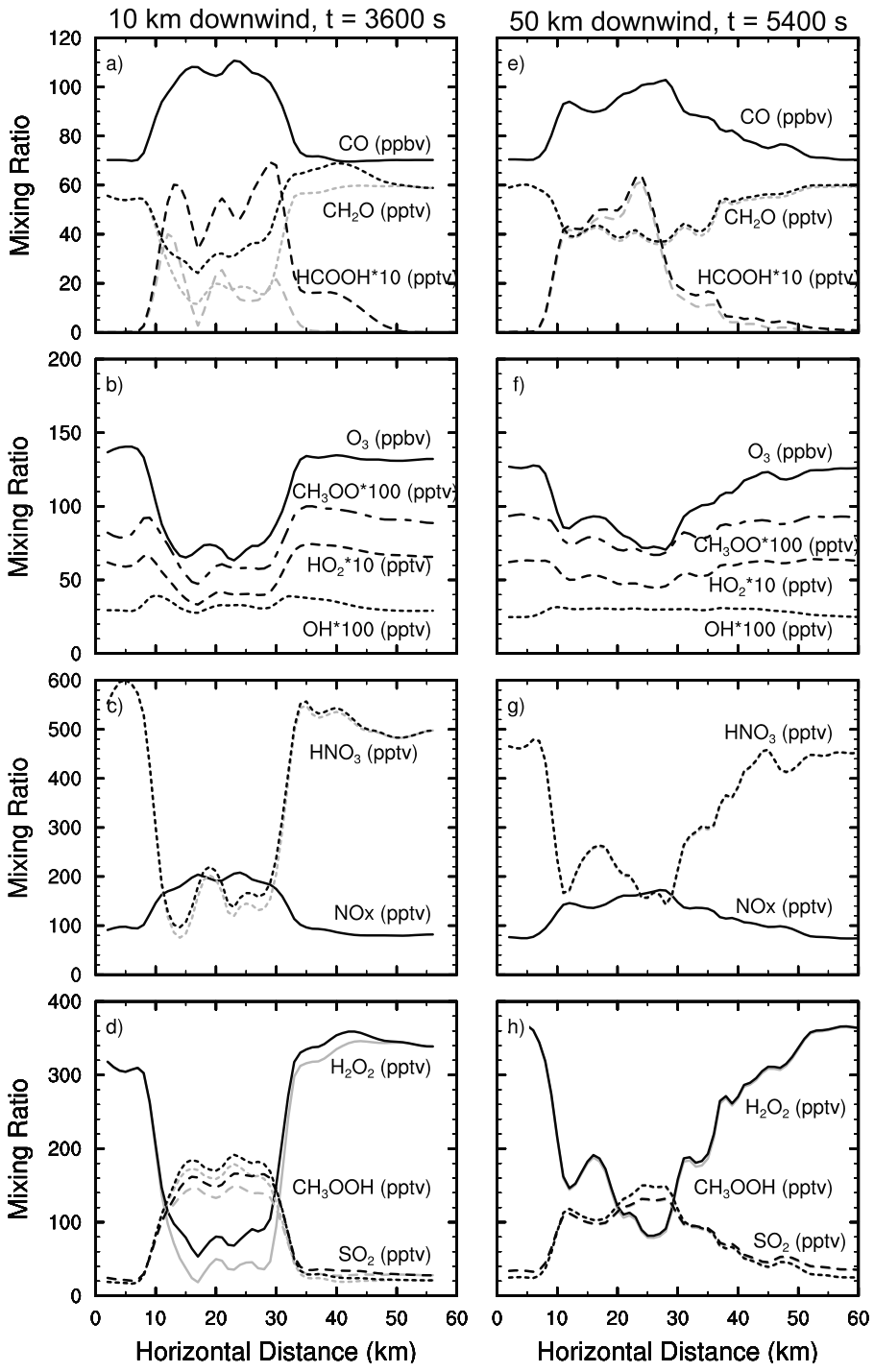

Figure 6. Modeled species mixing ratio along the transects plotted in Figure 5. (a–d) t = 3600 s at 10 km downwind (line C-D) of southeasternmost storm core. (e–h) t = 5400 s at 50 km downwind (line G-H) of storm core. Black lines are total mixing ratios, gray lines are gas-phase mixing ratios. Results are from the pH-Calc (control) simulation.

ratios reported by *Li et al.* [1994] are 16 ± 4 pptv/ppbv for a ground site in rural Ontario, Canada, sampled in July–September 1988. Ratios determined from the NASA INTEX-A field program, which occurred over the eastern 2/3 of the continental United States during July 2004, are 13.7 ± 9.1 pptv/ppbv in the boundary layer and 1.5 ± 1.6 pptv/ppbv between 10 and 12 km mean sea level (A. Fried, personal communication). The ratios from our simulations are low compared to observations because of the lack of nonmethane hydrocarbon chemistry included in the model. Nevertheless, the simulated ratios are within the large uncertainty calculated for the INTEX-A data.

[30] Figures 7 and 8 show that formaldehyde is not completely in the gas phase but also can be found in the

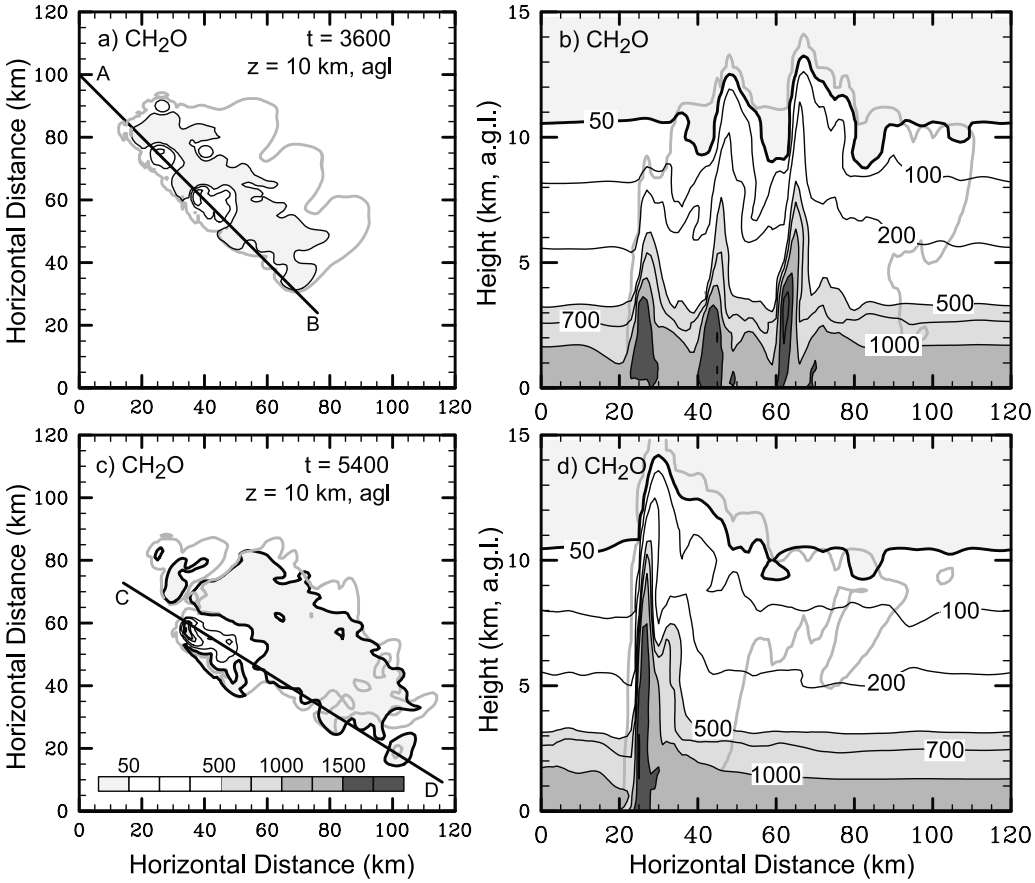

Figure 7. Horizontal and vertical cross sections of simulated total (= gas + cloud water + rain + ice + snow + hail) CH_2O (pptv = pmol (mol air)$^{-1}$) at (a and b) t = 3600 s and at (c and d) t = 5400 s from the pH-Calc (control) simulation. The vertical cross sections are along the storm axis (indicated by lines A-B and C-D in the horizontal cross sections). Contours are 50, 100, 200, 500, 700, 1000, 1500, and 2000 pptv. The gray line is the total condensate mixing ratio equal to 0.01 g kg^{-1}.

liquid and ice hydrometeors. To exemplify the distribution of formaldehyde among the water reservoirs, the same vertical cross section along the storm axis of formaldehyde is illustrated (Figure 9). In the lower region of the storm (the total condensate q_{tot} = 0.01 g kg^{-1} isoline marks the storm), formaldehyde mixing ratios reach 1000 pptv in the gas phase, rain, and hail. Above 6 km a.g.l., significant amounts of CH_2O are in the snow and hail reservoirs. In this cross section, CH_2O in hail reaches values of 1000 pptv which is much higher than CH_2O in any of the other cloud hydrometeors. The riming process (snow and hail collecting cloud water and rain) are the dominant pathways for transferring dissolved formaldehyde (and all dissolved species) to the frozen hydrometeors. The magnitude of these hail CH_2O mixing ratios critically depend on the microphysics parameterization used and on the assumption that soluble species are retained in frozen drops. Because of uncertainties in the microphysics parameterization and in the retention of species in freezing drops, the results shown here also contain some uncertainty (discussed in section 5).

[31] To further quantify the distribution of formaldehyde among the cloud hydrometeors, the sum of formaldehyde in each hydrometeor is calculated relative to the total amount of formaldehyde in all the hydrometeors for the entire model domain (Figure 10a). Early in the simulation, during the multicell stage of the storm, CH_2O mostly resides in the rain and hail hydrometeors. During the transition from the multicell to the supercell stage (80 < t < 120 min) of the storm, CH_2O in snow and hail are the largest fractions of CH_2O in the condensed phase. After t = 120 min (supercell stage), CH_2O mostly resides in the snow, hail, and rain.

[32] Except for hail, the traces of the formaldehyde in each hydrometeor do not mimic the traces of the cloud particles themselves (Figure 11). The percent of snow in the total condensate is large during the multicellular stage of the simulated storm while the percent of CH_2O in snow is not large until the transition stage. The percent of rain is much smaller than the percent of CH_2O in rain during the multicellular stage. These results indicate that microphysical conversion from cloud water directly to rain is more important during the multicellular stage of the simulated storm than the supercell stage, and the dissolved species are likewise affected.

[33] The percentage of CH_2O in each cloud hydrometeor and in the gas phase is also calculated for the anvil region. The anvil is defined as the region where the maximum reflectivity in a grid point column is less than 40 dBZ and snow mixing ratios are greater than 10^{-7} kg kg^{-1}. Within

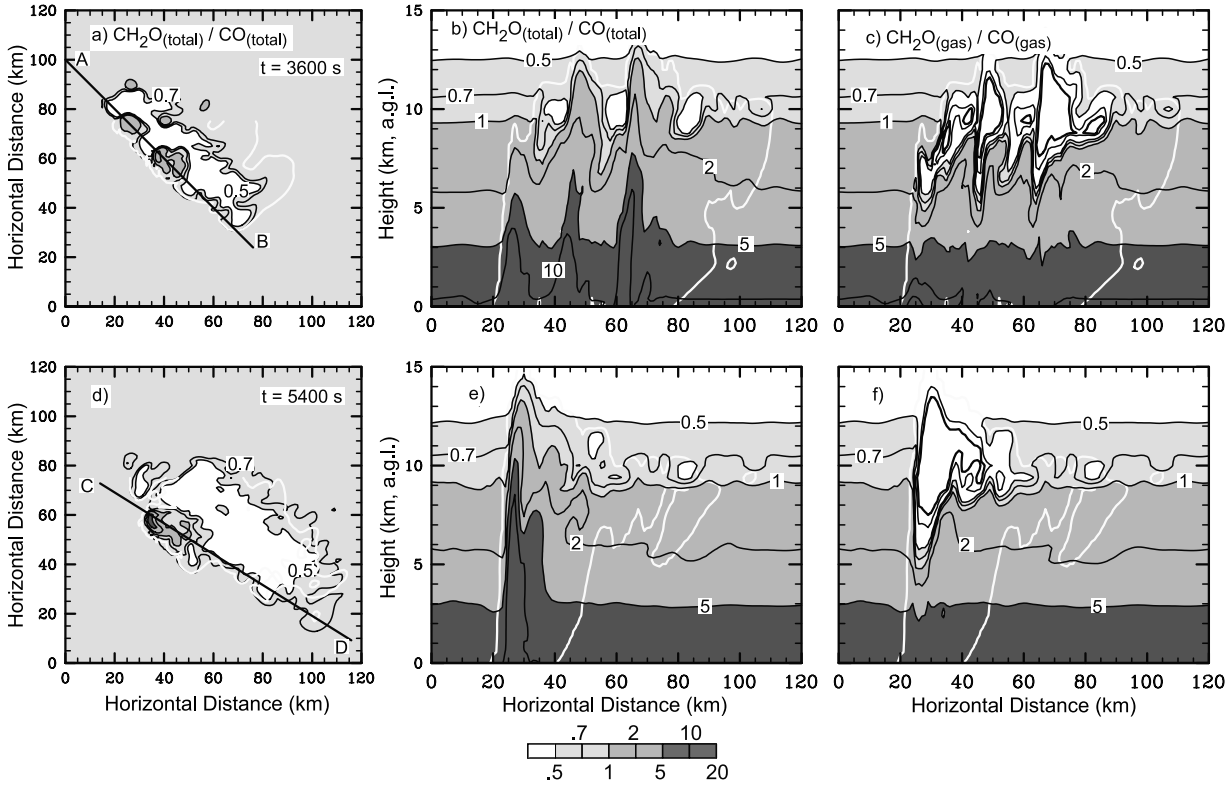

Figure 8. Ratio (pptv/ppbv) of CH_2O to CO at (a–c) t = 3600 s and at (d–f) t = 5400 s from the pH-Calc (control) simulation. Horizontal cross sections (Figures 8a and 8d) of the total ratio are at 10 km a.g.l. Vertical cross sections along the storm axis (indicated by the A-B and C-D lines in the horizontal cross sections) of total CH_2O to total CO ratio (Figures 8b and 8e) and of gas-phase-only CH_2O to gas-phase-only CO ratio (Figures 8c and 8f). Contours are 0.1, 0.2, 0.5, 0.7, 1.0, 2.0, 5.0, 10.0 pptv/ppbv. The white line is the total condensate mixing ratio equal to 0.01 g kg^{-1}.

the anvil, CH_2O is mostly in the gas phase (Table 6), with the remainder being primarily in the snow. Formaldehyde is mostly in the gas phase within the storm anvil because only a small amount of CH_2O resides in the snow compared to the gas phase (compare Figures 9e and 9a) and because the snow falls into regions of relatively higher gas-phase formaldehyde mixing ratios. One process not simulated here, the adsorption of gas-phase CH_2O onto the ice and snow, could alter the partitioning between gas and ice phases in the anvil. Depending on the ice surface area, formaldehyde should have some adsorption occurring [*Winkler et al.*, 2002; *Wang*, 2005].

[34] The distributions of total formaldehyde from each of the simulations conducted are quite similar to those shown for the control simulation (Figure 7) except for the Degassed simulation which has more formaldehyde in the convective outflow. When dissolved species are degassed during drop freezing, the species is then able to be transported to the upper troposphere [*Barth et al.*, 2001]. The No-Chem simulation has more CH_2O in the boundary layer and updraft region of the storm because it is not chemically destroyed. Small differences are found among the other simulations such as in the L(NOx)-On simulation more CH_2O exists at z = 9–10 km a.g.l. 40–60 km downwind of the storm core. In the No-AqChem simulation, there is a small increase in CH_2O at z = 10 km a.g.l. 20–30 km downwind of the storm core because aqueous-phase destruction of CH_2O reduces the transport of the species to higher altitudes. The percentage of CH_2O in each hydrometeor reservoir (Figure 10) shows that, in general, CH_2O is partitioned similarly in each simulation except the Degassed simulation. These conclusions are also true for the partitioning of CH_2O in the anvil between the gas and snow (Table 6). Additional differences between the simulations are discussed below in the context of scavenging efficiencies and fluxes to the upper troposphere.

4.4. Formic Acid as a Tracer of Cloud Processed Air

[35] Carboxylic acids are found in the atmosphere in very low concentrations because their primary gas-phase source is very small. HCOOH is produced in the gas phase by oxidation of hydrocarbons such as isoprene [*Helas et al.*, 1992; *Sanhueza et al.*, 1996], which is not included in these simulations, and destroyed in the gas phase by reaction with OH (G27). Formic acid is also formed in the aqueous phase by formaldehyde oxidation (A8) [*Chameides*, 1984] and is destroyed by reaction with OH (A4-A5). Thus, formic acid can reach a steady state concentration in the cloudy atmosphere [*Chameides*, 1984; *Barth et al.*, 2003]. Here we discuss the distribution of formic acid produced by aqueous-phase chemistry in deep convection. These results should indicate the viability of using HCOOH measurements to detect cloud-processed air. However, these results are based on the assumption that there is no background formic acid

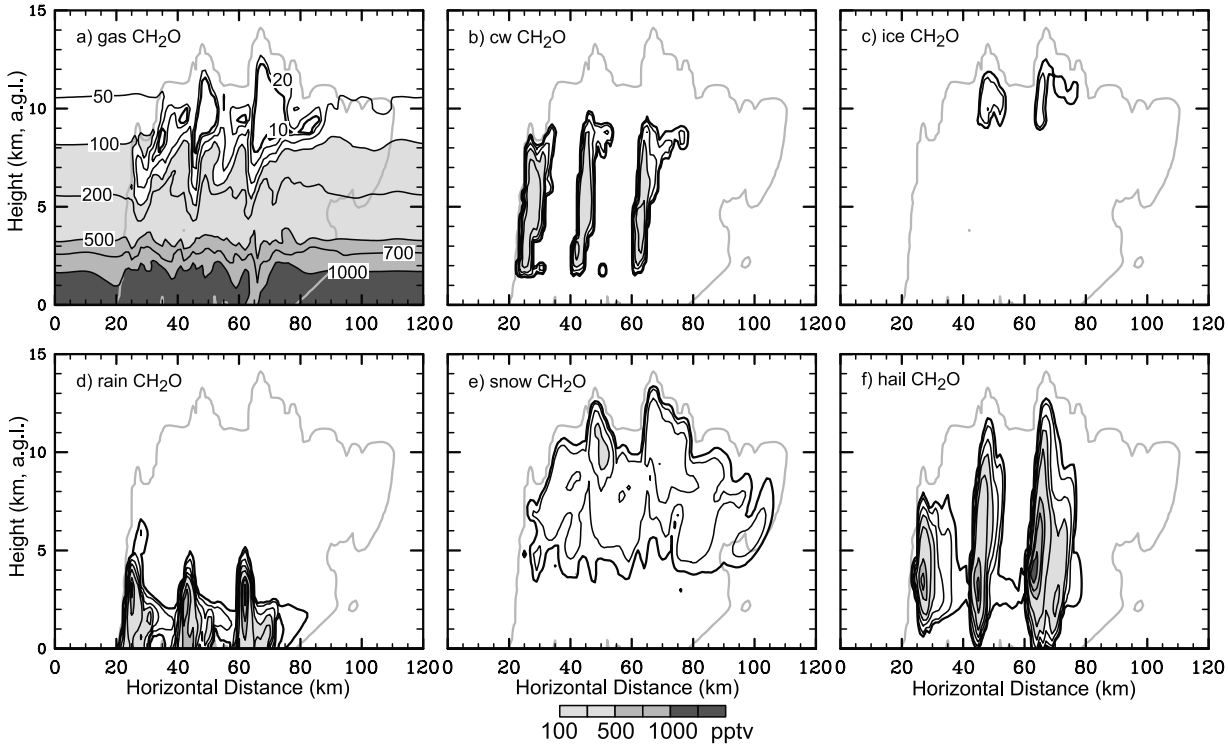

Figure 9. Vertical cross section (indicated by line A-B in the horizontal cross section of Figure 8) of CH_2O in the (a) gas phase, (b) cloud water, (c) ice, (d) rain, (e) snow, and (f) hail at $t = 3600$ s from the pH-Calc (control) simulation. Contours are 10, 20, 50, 100, 200, 500, 700, 1000, and 1500 pptv. The gray line is the total condensate mixing ratio equal to 0.01 g kg^{-1}.

before convection is initiated. Although isoprene levels in the Colorado-Wyoming-Nebraska region are near zero indicating HCOOH may also be near zero, other hydrocarbons do exist which may produce some HCOOH. By setting initial HCOOH to 0, we can track the location of the air that came in contact with the liquid regions of the storm. Thus, formic acid serves as a tracer of cloud-processed air within the simulation framework.

[36] Horizontal and vertical cross sections of total HCOOH mixing ratios are shown in Figure 12. The largest mixing ratios (~100 pptv) are found in the storm core where the cloud water is located. Much smaller mixing ratios (<20 pptv) are found in the convective outflow. While it is possible to measure such low concentrations of gas-phase HCOOH, measurements of HCOOH may not be the most reliable method of detecting cloud-processed air masses that cover small regions.

[37] The sum of formic acid in each hydrometeor is calculated relative to the total amount of formic acid in all the hydrometeors for the entire model domain (Figure 13). Results from the No-AqChem and No-Chem simulations are not presented because HCOOH = 0 throughout the simulations (initial HCOOH is 0 and HCOOH production occurs only in the aqueous phase). Because the source of HCOOH is in the cloud water, partitioning among the hydrometeors differs from that for CH_2O. Approximately 60% of the HCOOH in the condensed phase is in the snow at the end of the simulation, compared to 40% of the CH_2O in the condensed phase. The fraction of HCOOH in hail (10–20%) is much less than that found for CH_2O in hail (20–35%). More HCOOH in snow is also found in the anvil region (Table 6) compared to the CH_2O partitioning in the anvil. Results from the sensitivity simulations show small differences in HCOOH mixing ratios and the percentage of HCOOH in each hydrometeor reservoir (Figure 13) between the pH-Calc and pH = 4.5 simulations. These differences illustrate the sensitivity of HCOOH chemistry to the pH value in the cloud water and rain. When HCOOH is degassed during drop-freezing processes, its total mixing ratio in the convective outflow reaches 100 pptv, much greater than that found in the pH-Calc simulation (Figure 12). The L(NOx)-On simulation produces very similar HCOOH results (Figure 13) to those from the pH-Calc simulation as would be expected.

4.5. Hydrogen and Methyl Hydrogen Peroxide

[38] Hydrogen peroxide is a reservoir species for hydrogen oxide radicals (OH and HO_2) and is an important oxidant for aqueous-phase sulfur chemistry. It is produced in the gas phase primarily through the self reaction of hydroperoxy radicals (HO_2, G7) and is destroyed via photodissociation (G8) or reaction with OH (G9). In the aqueous phase, H_2O_2 is formed by HO_2 reacting with its anion, O_2^- (superoxide, A9), and is destroyed primarily by bisulfite ion (HSO_3^-, A13). The gas-phase source of methyl hydrogen peroxide is reaction of methylperoxy radical (CH_3OO) with HO_2 (G18). Like H_2O_2, methyl hydrogen peroxide is destroyed via photodissociation (G21) and via reaction with OH in the gas phase (G22). CH_3OOH has a much smaller solubility than H_2O_2 but can still dissolve into

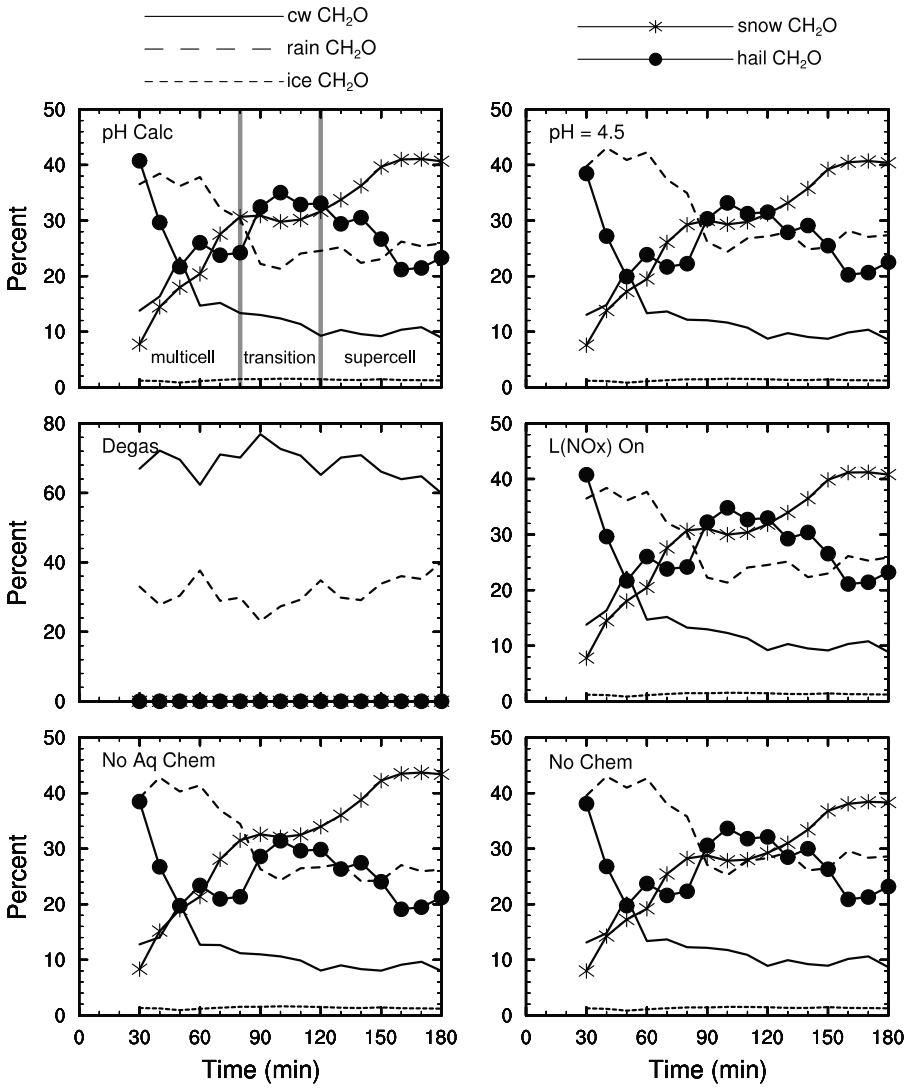

Figure 10. Percent of CH_2O in each hydrometeor reservoir relative to the total amount of CH_2O in all the hydrometeor reservoirs over the model domain as a function of time in the simulation sampled every 10 min. Results are for (a) the simulation where pH is calculated, (b) the simulation where pH is prescribed to 4.5, (c) the simulation where soluble species are degassed during drop freezing, (d) the simulation which includes NO_x production by lightning, (e) the simulation where aqueous chemistry does not occur, and (f) the simulation with no gas or aqueous chemistry.

water then react in the aqueous phase with OH (A7-A8). Because of the significant difference in solubility between H_2O_2 and CH_3OOH (at $T = 298$ K, Henry's law coefficient of H_2O_2 is 8.33×10^4 and CH_3OOH is 311 M atm^{-1}), the reduction in the ratio of H_2O_2 to CH_3OOH can indicate cloud processing [*Heikes et al.*, 1996; *Pickering et al.*, 1996; *Cohan et al.*, 1999; *Kim et al.*, 2002].

[39] Vertical cross sections of total H_2O_2 and CH_3OOH (Figure 14) show that CH_3OOH is primarily transported by convection while H_2O_2 is scavenged and removed from the atmosphere. Total H_2O_2 in the anvil region of the storm is substantially reduced (<200 pptv compared to the boundary layer mixing ratio of ~2500 pptv and the unperturbed UT mixing ratio of 200–500 pptv). This contrasts with the H_2O_2 measurements reported for tropical oceanic convection (which generally has more liquid than the continental midlatitude storms) sampled in PEM Tropics A [*Cohan et al.*, 1999] that showed higher convective outflow mixing ratios (330 ± 140 pptv) compared to the unperturbed UT (200 ± 110 pptv). CH_3OOH in the convective outflow has values >100 pptv compared to its boundary layer mixing ratio of 300–500 pptv and its unperturbed UT mixing ratio of 20–50 pptv. These values are similar to those reported by *Cohan et al.* [1999]. Within the storm core, the ratio of total H_2O_2 to total CH_3OOH (Figure 15) is similar to that found in the boundary layer. The total ratios within the storm core are ~5 compared with ~2 in the convective outflow and >10 in the background upper troposphere. The gas-phase H_2O_2 to gas-phase CH_3OOH ratios are substantially reduced to values <0.1 within the core(s) of the storm where H_2O_2 has partitioned to cloud water, rain, and hail. Because the H_2O_2 in rain and hail are removed via precipitation, these low gas-phase ratios are not found in the convective outflow where these ratios are quite variable, ranging from 1 to 7. *Heikes et al.* [1996] reported enhanced H_2O_2 to CH_3OOH ratios in the UT when SO_2 mixing ratios

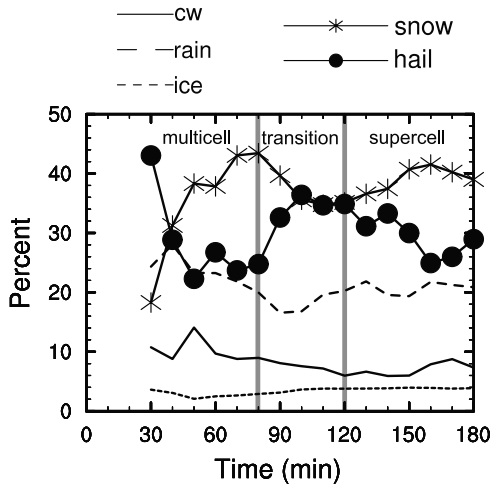

Figure 11. Percent of each hydrometeor reservoir relative to the total amount of condensed water over the model domain as a function of time in the simulation sampled every 10 min.

were low (<100 pptv) and reduced ratios when SO_2 mixing ratios were >100 pptv indicating the importance of aqueous-phase chemistry on H_2O_2. The reduced ratios reported by *Heikes et al.* [1996] were ~0.7. Measurements of convective outflow during TRACE A over South America indicated H_2O_2 to CH_3OOH ratios of ~1 in fresh convective outflow and >2 in aged convective outflow which underwent photochemistry [*Pickering et al.*, 1996]. *Cohan et al.* [1999] found substantially reduced gas-phase ratios in fresh convective outflow of <1 compared to UT background values of 2–5 for the tropical South Pacific, indicating significant scavenging of H_2O_2 by deep convection. On the other hand, for nonprecipitating clouds, *Kim et al.* [2002] calculated gas-phase ratios after cloud encounter of 1.7 compared with values of 2 in clear sky for NO_x mixing ratios of 50 pptv (similar to the UT region of this study). Our results are similar to these previous results in that the H_2O_2 to CH_3OOH ratio is reduced after convective processing. However, *Cohan et al.* [1999] reported a greater reduction of the ratio, likely because of different types of convection (marine tropical convection with less ice versus continental midlatitude convection with more ice and low SO_2 mixing ratios) or analysis approaches. We found a greater reduction (from 10 in UT to 1–7 in convective outflow, Figures 15c and 15f) after convection than reported by *Kim et al.* [2002] because of the precipitation that removes H_2O_2 in our study.

[40] The partitioning of H_2O_2 among the cloud hydrometeors is similar to that found for CH_2O (Figure 9). H_2O_2 mixing ratios can be found mostly in the gas phase, in the rain, and in the hail below ~6-km altitude. At higher altitudes, H_2O_2 is in the gas phase and in the snow. As with CH_2O, the magnitude of H_2O_2 in the ice, snow and hail depends on the microphysics parameterization and the assumption that dissolved H_2O_2 is retained in the frozen hydrometeors (discussed in section 5).

[41] The partitioning of H_2O_2 among the cloud hydrometeors is further quantified by calculating the relative amount of H_2O_2 in each hydrometeor to the total amount of H_2O_2 in all the hydrometeors for the model domain (Figure 16). Results show that during the multicell stage of the storm ($t < 80$ min) the H_2O_2 resides primarily in the rain, hail, and the cloud water hydrometeors. At later times (during the supercell stage of the storm), H_2O_2 resides in the snow, rain, and hail.

[42] The relative amount of H_2O_2 and CH_3OOH in each cloud hydrometeor and in the gas phase is also calculated for the anvil region. Within the anvil, 92–95% of H_2O_2 is in the gas phase (Table 6), with the remaining H_2O_2 being in the snow. Despite the vastly different Henry's law coefficients for H_2O_2 and CH_3OOH, the relative amount of CH_3OOH in the gas phase is the same as that for H_2O_2. The high percentage of H_2O_2 in the gas phase is due to two factors, (1) similar in-snow mixing ratios (~300 pptv) relative to gas-phase mixing ratios but over a smaller region for in-snow and (2) the fallout of snow into regions of relatively higher gas-phase H_2O_2 mixing ratios. Again, the adsorption of gas-phase peroxides onto the ice and snow could alter the partitioning in the anvil region.

[43] The distributions of total hydrogen peroxide from each of the simulations conducted except the Degassed simulation are similar to that found in the pH-Calc simulation (Figure 14). All the simulations except the Degassed simulation have negligible amounts of boundary layer H_2O_2 reaching the upper troposphere indicating that the ice microphysical processes are important to the wet deposition of H_2O_2. In the core of the storm, aqueous chemistry acts to reduce H_2O_2 mixing ratios as seen by the higher mixing ratios in the No-AqChem and No-Chem simulations compared to the pH-Calc simulation. The differences (which are small) between these simulations are also seen in the percentage of H_2O_2 in each hydrometeor reservoir (Figure 16). H_2O_2 is slightly reduced in the storm core when production of NO_x by lightning is included in the simulation.

[44] Total methyl hydrogen peroxide mixing ratio distributions from each simulation (Figure 17) at $t = 5400$ s also shows that more CH_3OOH reaches the upper troposphere

Table 6. Percent of CH_2O, HCOOH, H_2O_2, and CH_3OOH in the Gas Phase and in the Snow Hydrometeors Within the Anvil Region for $t = 60$–180 min of the Simulations

	CH_2O		HCOOH		H_2O_2		CH_3OOH	
Simulation	Gas	Snow	Gas	Snow	Gas	Snow	Gas	Snow
pH-Calc	88–92	7–9	45–72	25–46	92–95	4–6	93–95	4–6
pH = 4.5	88–91	7–9	50–76	22–41	92–96	4–6	93–95	4–6
Degassed	99–100	0	99–100	0	99–100	0	100	0
L(NOx) on	89–93	6–9	45–72	25–46	92–95	4–6	93–95	4–6
No-AqChem	86–90	9–11	–	–	92–95	4–6	93–95	4–6
No-Chem	86–89	9–12	–	–	92–95	4–6	92–95	4–7

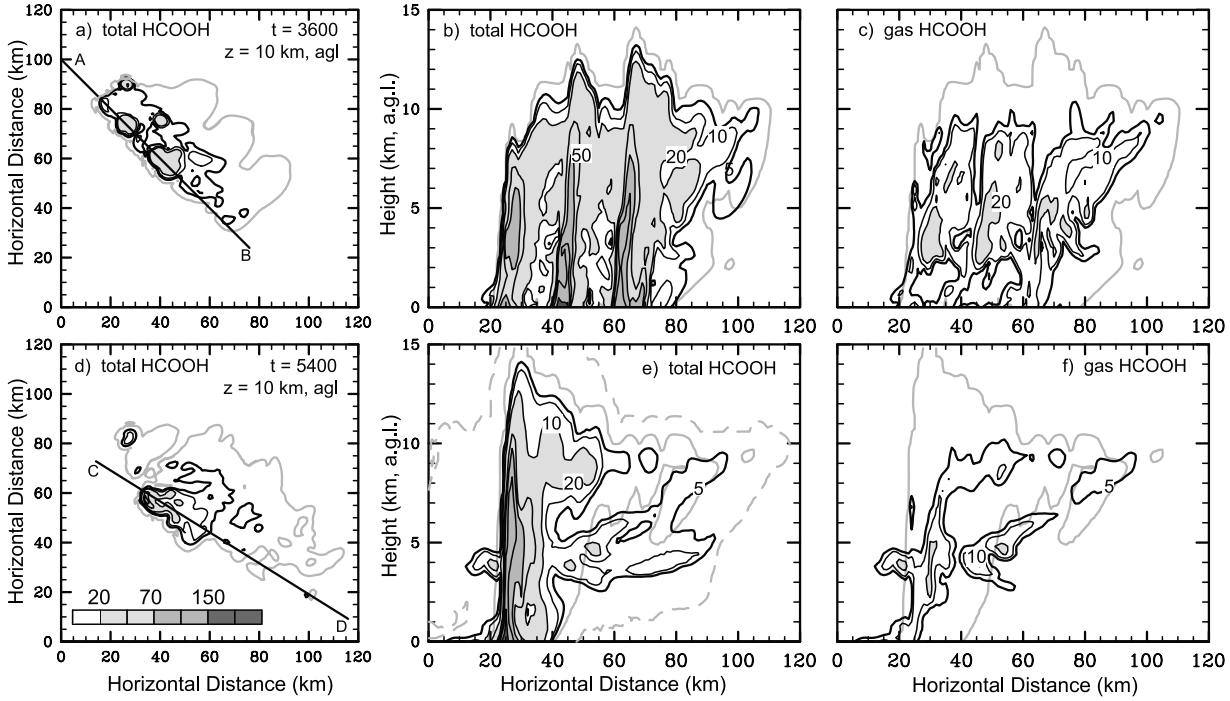

Figure 12. Horizontal and vertical cross sections of simulated HCOOH (pptv = pmol (mol air)$^{-1}$) at (a–c) t = 3600 s and at (d–f) t = 5400 s from the pH-Calc (control) simulation. The cross sections are along the storm axis (indicated by the lines in the horizontal cross sections). Figures 12a, 12b, 12d, and 12e are total HCOOH, Figures 12c and 12f are gas-phase HCOOH. Contours are 5, 10, 20, 50, 70, 100, 150, and 200 pptv. The solid and dashed gray lines are the total condensate mixing ratio equal to 0.01 and 10^{-6} g kg^{-1}, respectively.

when dissolved species degas during drop freezing than when the dissolved species is retained. The distribution produced in the No-Chem simulation shows that CH_3OOH mixing ratios are affected by gas-phase chemistry. However, aqueous chemistry has only a small effect on CH_3OOH mixing ratios in the storm core and no effect outside the core. There are also slightly smaller CH_3OOH mixing ratios when NO_x is produced from lightning in the storm core.

5. Discussion

5.1. Scavenging Efficiency

[45] The scavenging efficiency for a species can be characterized in a variety of ways. These methods include first-order removal rates [*Giorgi and Chameides*, 1986], comparing the concentration of a species in the precipitation to that in the boundary layer air, comparing the flux of species in the precipitation to the flux of that species entering the storm [*Easter and Hales*, 1983], and a two-component mixture method [*Cohan et al.*, 1999]. Here we define the scavenging efficiency of a species as the ratio of the rate of the species deposition in the precipitation at the surface to the rate of species ingestion into the storm. The rate of ingestion (F_{in}, mol s^{-1}) into the storm is found by calculating the upward vertical flux divergence of the species from 500 m above ground to cloud base, that is

$$F_{in} = \int_{500m}^{cloudbase} \int_{\Omega} \left. \frac{\partial(\overline{\rho} w C_{gas})}{\partial z} \right|_{forw>0} d\Omega dz \qquad (1)$$

where Ω is the horizontal domain [*Skamarock et al.*, 2000], $\overline{\rho}$ is the base state density, w is vertical velocity. For this calculation, C_{gas} is in units of moles per kilogram air. This scavenging efficiency calculation neglects ingestion of the species on the sides of the storm core due to entrainment but should give a reasonable estimate since the species discussed below have higher concentrations in the boundary layer than in the free troposphere. The scavenging efficiency for each simulation is integrated from t = 0 to 180 min (Table 7).

[46] The magnitude of the scavenging efficiency is affected by a number of factors including the solubility of the species but also the cloud processes occurring within and below the cloud. Evaporation of raindrops below cloud would reduce scavenging efficiencies, similar to reducing precipitation efficiencies. Another factor that affects the scavenging efficiency is the residence time the species is in contact with the liquid phase. *Barth et al.* [2001] estimated that the air parcel spends about 400–700 s in contact with liquid water for the 10 July 1996 STERAO storm. This short residence time may limit the amount of species scavenged by the cloud drops. Storms with deeper convective cores (and liquid water regions) or with smaller updraft velocities may be more efficient in scavenging soluble species.

[47] Similar scavenging efficiencies for CH_2O of 46% are found for the pH-Calc and L(NOx)-On simulations. Significantly more CH_2O is scavenged when the pH = 4.5 and when aqueous chemistry does not occur (No-AqChem and No-Chem). Significantly less CH_2O is scavenged when the

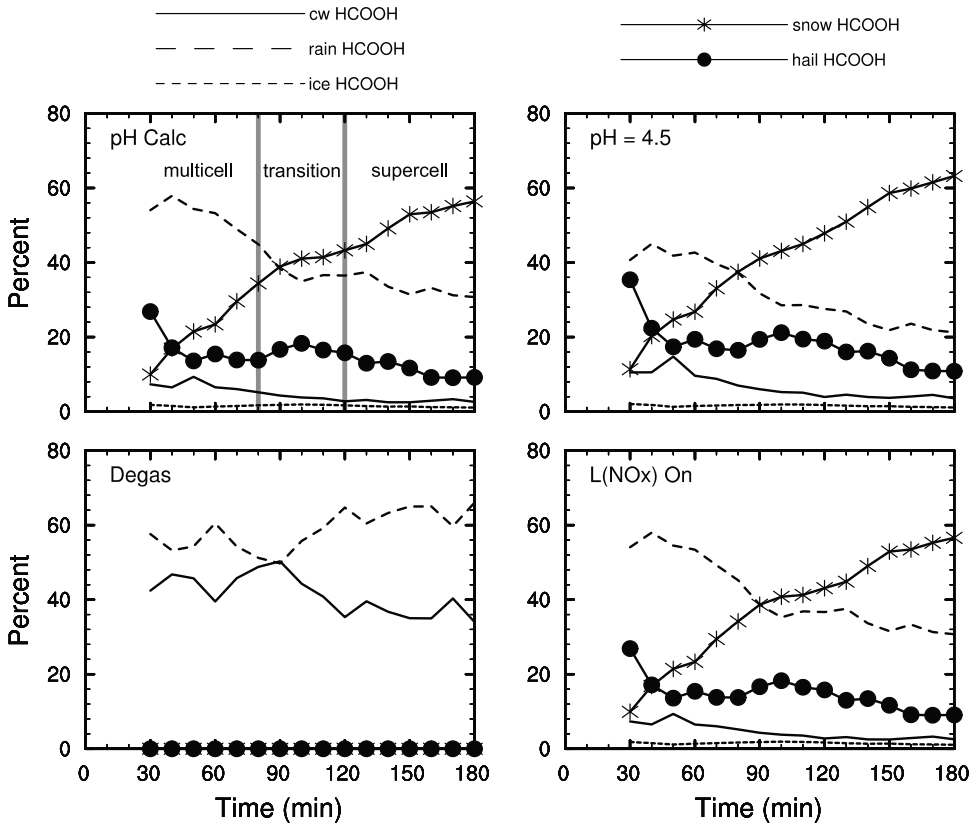

Figure 13. Percent of HCOOH in each hydrometeor reservoir relative to the total amount of HCOOH in all the hydrometeor reservoirs over the model domain as a function of time in the simulation sampled every 10 min. Results are for (a) the simulation where pH is calculated, (b) the simulation where pH is prescribed to 4.5, (c) the simulation where soluble species are degassed during drop freezing, and (d) the simulation which includes NO_x production by lightning.

CH_2O degasses during cloud drop freezing, showing the importance of microphysical processes in enabling the wet deposition of soluble species. The ratio of the removal rate of CH_2O + HCOOH in the precipitation to the flux of CH_2O+ HCOOH into the storm has scavenging efficiencies of 60–67% for all the simulations that retain soluble species in frozen hydrometeors during drop freezing. Although the scavenging efficiency of CH_2O in the pH-Calc simulation is much less than its value in the pH = 4.5 simulation, the scavenging efficiency of CH_2O + HCOOH in the pH-Calc simulation is closer to that in the pH = 4.5 simulation, indicating that the pH plays an important role in partitioning these two species. The calculated pH ranges from 4.19 to 4.39 for the cloud water and from 4.27 to 4.53 for the rainwater. At lower pH, the partitioning between $HCOO^-$ and HCOOH in the aqueous phase favors HCOOH (aqueous). However, HCOOH is destroyed more slowly than $HCOO^-$ (A4 and A5, Table 3). Thus, at lower pH, total formic acid has larger concentrations than at higher pH values. Consequently, more total formic acid is available for scavenging.

[48] The scavenging efficiencies calculated for H_2O_2 are 55–58% for the pH-Calc, pH = 4.5, and L(NOx) simulations. Much less H_2O_2 is scavenged in the Degas simulation while more H_2O_2 is scavenged when the chemistry does not proceed, which indicates that chemistry is responsible for <10% of the H_2O_2 removal, however, gas and aqueous chemistry also produce H_2O_2. The H_2O_2 scavenging efficiency from the No-AqChem simulation is the same as that from the No-Chem simulation, indicating that gas-phase chemistry plays a minor role in the H_2O_2 budget. Compared to CH_2O and H_2O_2, CH_3OOH is hardly scavenged at all. Approximately 7% of the CH_3OOH entering the storm is removed via chemistry or precipitation.

[49] The scavenging efficiencies of HNO_3, NH_3, and total sulfur are also reported. Scavenging efficiencies for HNO_3 are about 96% for all the simulations except the Degas simulation for which it is 29%. HNO_3 does not undergo aqueous chemistry in the chemical mechanism used for these simulations, therefore there is little sensitivity of the HNO_3 scavenging in the No-AqChem simulation or the pH = 4.5 simulation. There is a small sensitivity to the No-Chem simulation. Chemistry of ammonia is not represented in these simulations, thus differences in scavenging efficiencies would be due to physical processes or pH concentrations of the drops. The ammonia scavenging efficiencies are 89% for all the simulations except the Degas simulation for which it is 32%. The scavenging efficiency for total sulfur calculated by combining SO_2 and SO_4^{2-} fluxes has more sensitivity among the different sensitivity simulations. The pH-Calc simulation scavenging efficiency is 59%. When there is no chemistry occurring, especially aqueous-phase chemistry, the sulfur scavenging efficiency drops to ~46%.

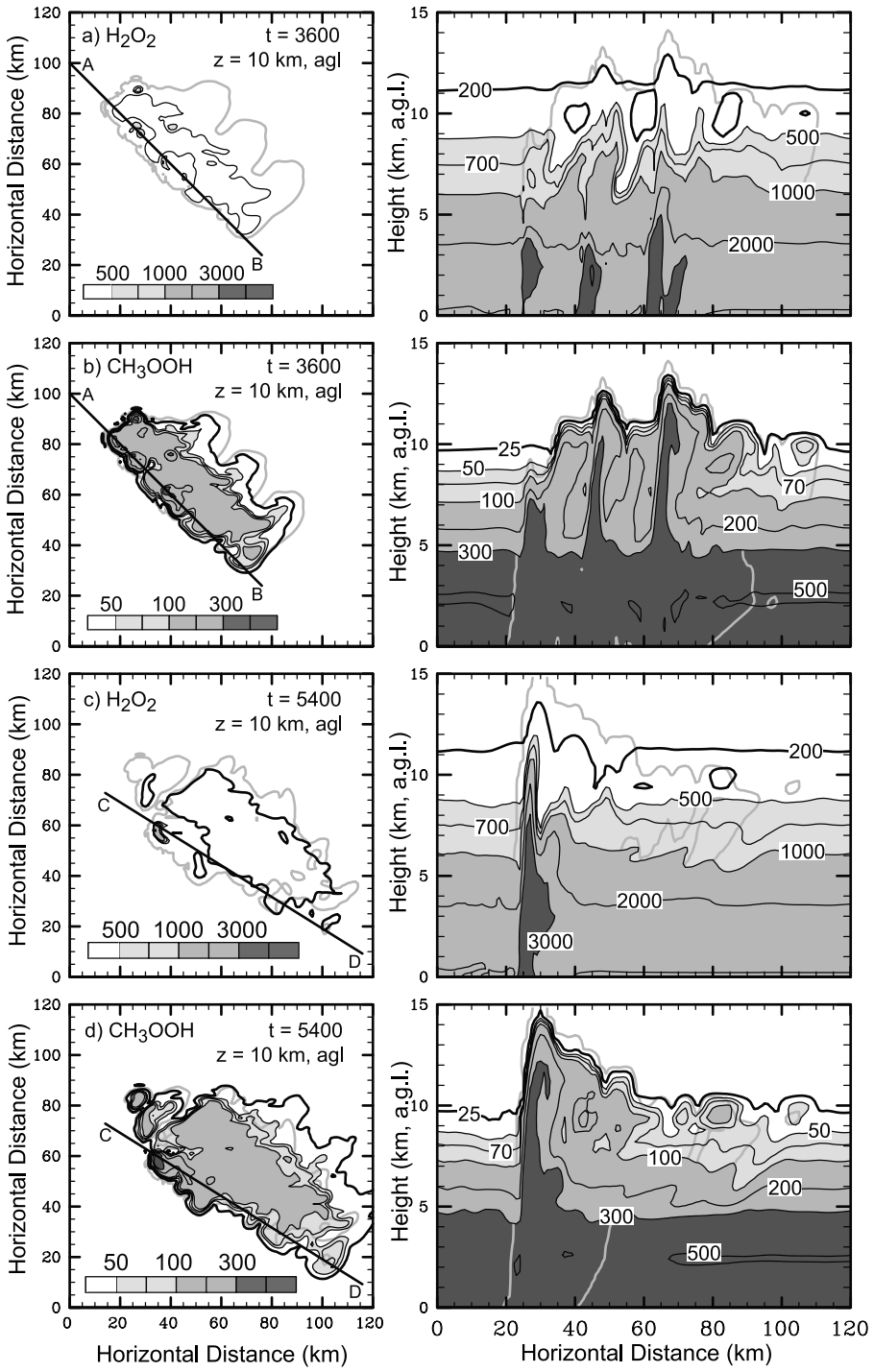

Figure 14. Horizontal (left column) and vertical (right column) cross sections of simulated total H_2O_2 (rows a and c) and total CH_3OOH (rows b and d) at t = 3600 s (rows a-b) and at t = 5400 s (rows c-d) from the pH-Calc (control) simulation. The cross sections are along the storm axis (indicated by the lines in the horizontal cross sections). Contours for H_2O_2 are 200, 500, 700, 1000, 2000, 3000, and 5000 pptv = pmol (mol air)$^{-1}$. Contours for CH_3OOH are 25, 50, 70, 100, 200, 300, 500 pptv. The gray line is the total condensate mixing ratio equal to 0.01 g kg^{-1}.

The aqueous sulfur chemistry is critical to the removal of sulfur from the atmosphere.

5.2. Net Flux to Upper Troposphere

[50] Vertical transport to the upper troposphere of the chemical species can be estimated by the vertical flux of each species. For a deep convective storm, the vertical fluxes F are determined as a combination of the advection flux and the precipitation flux, using the following equation:

$$F = \bar{\rho} w (C_{gas} + C_{cw} + C_r + C_i + C_s + C_h) + V_r \rho C_r + V_s \rho C_s + V_h \rho C_h \quad (2)$$

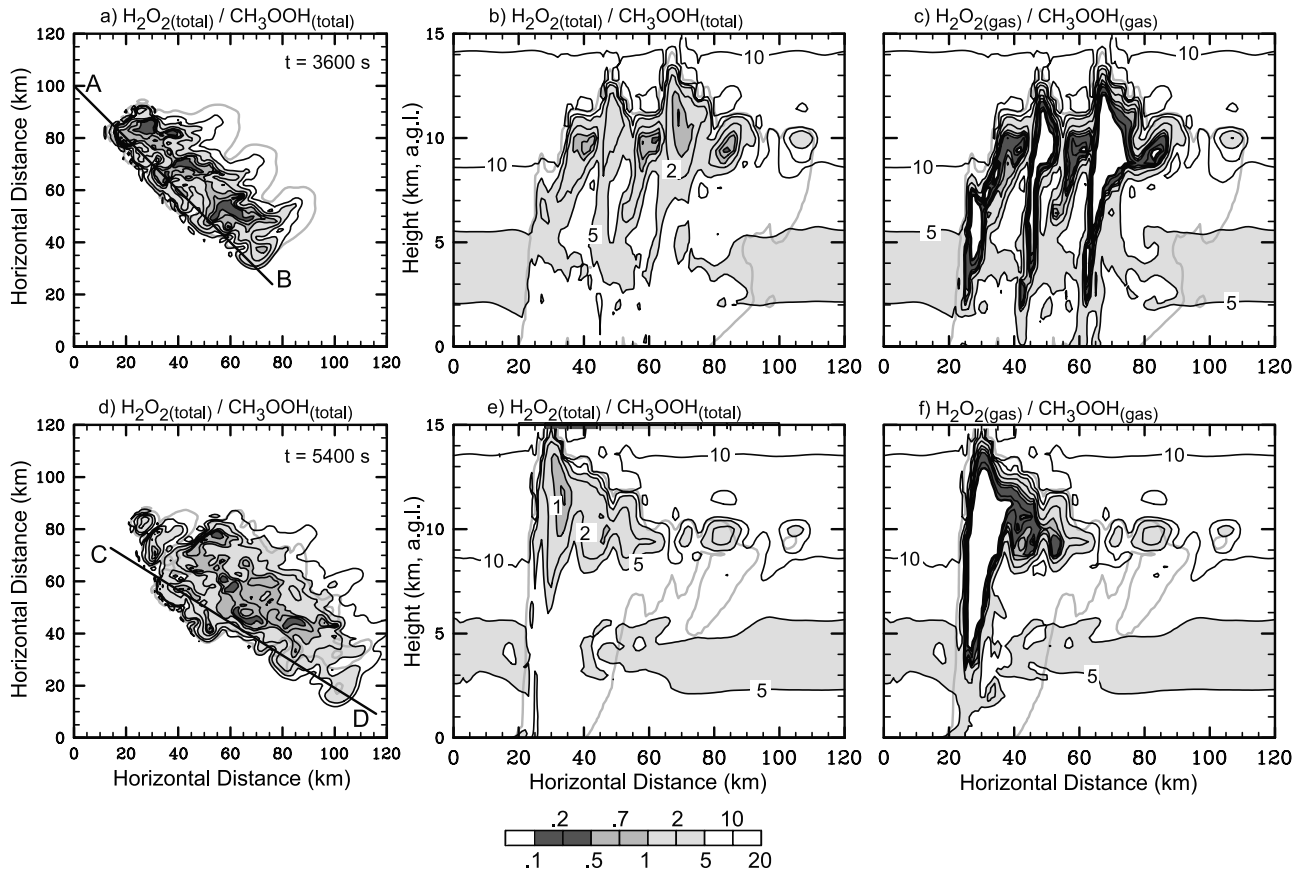

Figure 15. Ratio (dimensionless) of H_2O_2 to CH_3OOH at (a–c) $t = 3600$ s and at (d–f) $t = 5400$ s from the pH-Calc (control) simulation. Horizontal cross sections (Figures 15a and 15d) of the total ratio are at 10 km a.g.l. Vertical cross sections along the storm axis (indicated by the lines A-B and C-D in the horizontal cross sections) of total H_2O_2 to total CH_3OOH ratio (Figures 15b and 15e) and of gas-phase-only H_2O_2 to gas-phase-only CH_3OOH ratio (Figures 15c and 15f). Contours are 0.1, 0.2, 0.5, 0.7, 1, 2, 5, 10, and 20. The gray line is the total condensate mixing ratio equal to 0.01 g kg^{-1}.

where $\bar{\rho}$ is the air density, w is vertical velocity, C_{gas}, C_{cw}, C_r, C_i, C_s, C_h are the mixing ratio of the species in the gas phase, cloud water, rain, ice, snow, and hail, respectively, and V_r, V_s, V_h are the fallspeeds of rain, snow, and hail, respectively. These fluxes are calculated at each horizontal grid point every 500 m between the surface and 15 km a.g.l. and every 10 min from 30 to 180 min. The vertical fluxes are spatially averaged over the horizontal domain and temporally averaged over the 150-min period.

[51] The vertical fluxes are calculated for water vapor, nine species, and two families of species (Figure 18). The water vapor vertical flux is positive from the surface to ~10 km, with the greatest flux occurring below 5 km a.g.l. In contrast, the vertical flux for CO has its largest magnitude occurring in the midtroposphere (3–10 km a.g.l.). CO fluxes are not affected by the precipitation nor are they sensitive to the different simulations, indicating that it is controlled by convective transport. Ozone vertical fluxes are similar to CO but have a reduced peak above 5 km a.g.l. compared to the CO vertical fluxes and are negative above 17 km a.g.l. These fluxes show similarities with those reported by *Wang and Prinn* [2000] in the low level peak for water and the high level downward flux for ozone, which *Wang and Prinn* [2000] attribute to downward mixing of stratospheric ozone. However, the height of the maximum upward flux for CO and the magnitudes of the fluxes are smaller than those reported by *Wang and Prinn* [2000]. The difference in magnitude can be attributed to the size of the horizontal area that the vertical fluxes were calculated for. In this study, the entire model domain with large regions of small vertical flux is used for the flux calculation, while *Wang and Prinn* [2000] considered only the region of the convective cores. NO_x vertical fluxes are positive between the surface and 12 km a.g.l. The addition of the lightning source of NO_x increases its vertical flux above 6 km a.g.l. but decreases that flux below 6 km a.g.l. This is because of increased NO_x concentrations in the downdrafts. The vertical fluxes of the soluble species, CH_2O, CH_2O + HCOOH, H_2O_2, CH_3OOH, HNO_3, NH_3, SO_2, and SO_2+ SO_4^{2-}, exhibit different behavior that is sensitive to the configuration of the simulation. CH_2O, CH_2O + HCOOH, H_2O_2, HNO_3, and NH_3 have negative fluxes (indicating that they are removed by precipitation instead of transported to the upper troposphere) for all the simulations except the Degas simulation. Less soluble species, for example, CH_3OOH, are transported to the upper troposphere. Sensitivities to other simulations are less dramatic than those to the Degas simulation. The calculation

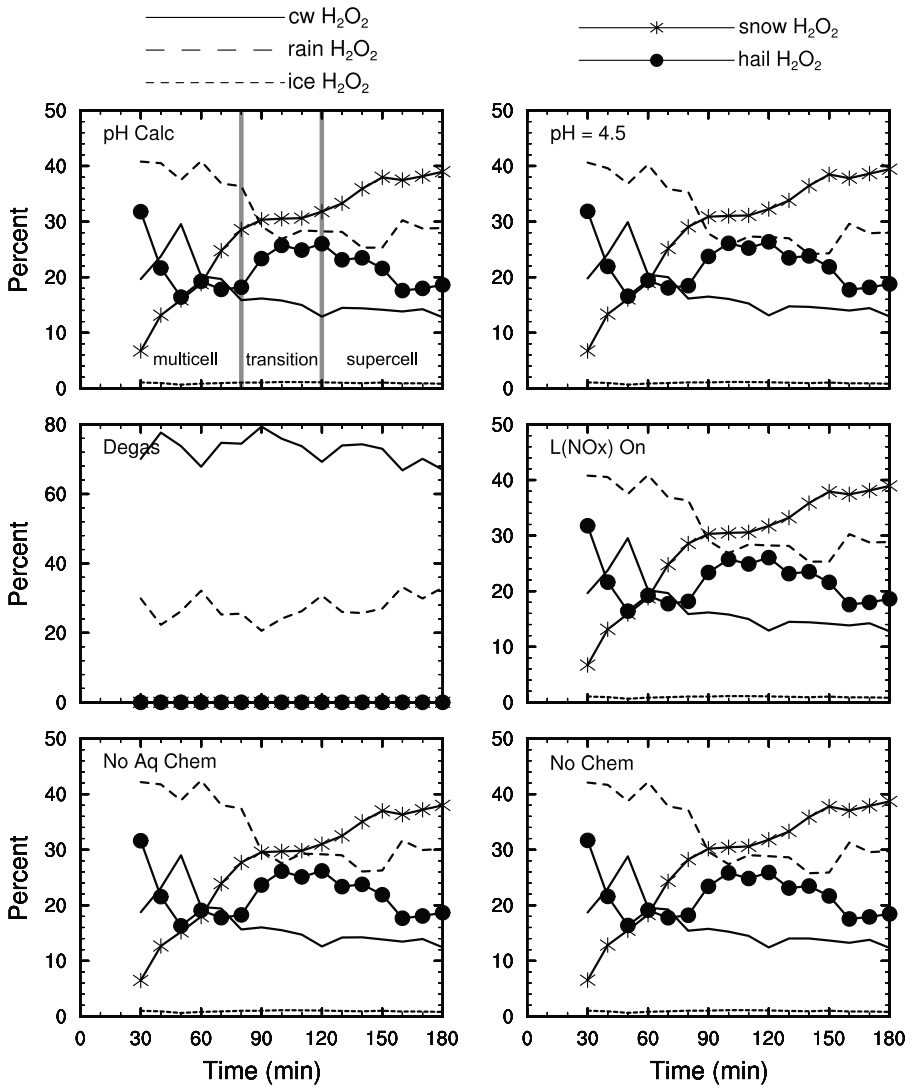

Figure 16. Percent of H_2O_2 in each hydrometeor reservoir relative to the total amount of H_2O_2 in all the hydrometeor reservoirs over the model domain as a function of time in the simulation sampled every 10 min. Results are for (a) the simulation where pH is calculated, (b) the simulation where pH is prescribed to 4.5, (c) the simulation where soluble species are degassed during drop freezing, (d) the simulation which includes NO_x production by lightning, (e) the simulation where aqueous chemistry does not occur, and (f) the simulation with no gas or aqueous chemistry.

of the pH is most important to SO_2 because of the strong pH dependence of the S(IV) + O_3 reaction. The inclusion of aqueous chemistry is important to the flux of SO_2 and $SO_2 + SO_4^{2-}$ but is a small factor to other species, in agreement with the work of *Wang and Prinn* [2000]. The No-Chem simulation indicates the importance of chemistry versus combined transport and precipitation scavenging. CO and O_3 are controlled by transport, HNO_3 and NH_3 are controlled by transport and precipitation scavenging, while the fluxes of the other species are altered by the gas phase and aqueous chemistry.

5.3. Implications for UT Composition and Chemistry

[52] Because ozone production in the UT depends on the magnitude of its precursors, NO_x and HO_x, it also depends on the source strength of the HO_x precursors, CH_2O, H_2O_2, and CH_3OOH [*Chatfield and Crutzen*, 1984; *Prather and Jacob*, 1997; *Jaeglé et al.*, 1997; *Wennberg et al.*, 1998; *Jaeglé et al.*, 2001]. Thus understanding the importance of various convective processes on the HO_x precursors is critical to understanding the influence of these species on UT ozone mixing ratios.

[53] Our model results show that most of the CH_2O and H_2O_2 ingested by the storm is removed by precipitation. The vertical fluxes of CH_2O and H_2O_2 are negative, thus CH_2O and H_2O_2 are removed from the UT. This is true for all the simulations except for the simulation in which the dissolved species is degassed during liquid drop freezing. For this sensitivity simulation, only 15% of the ingested CH_2O is rained out and a substantial amount of the ingested CH_2O is transported to the UT. *DeCaria et al.* [2005] calculate increases of CH_2O and H_2O_2 mixing ratios in the convective outflow of the modeled storm (12 July 1996 STERAO storm). However, their simulations are configured

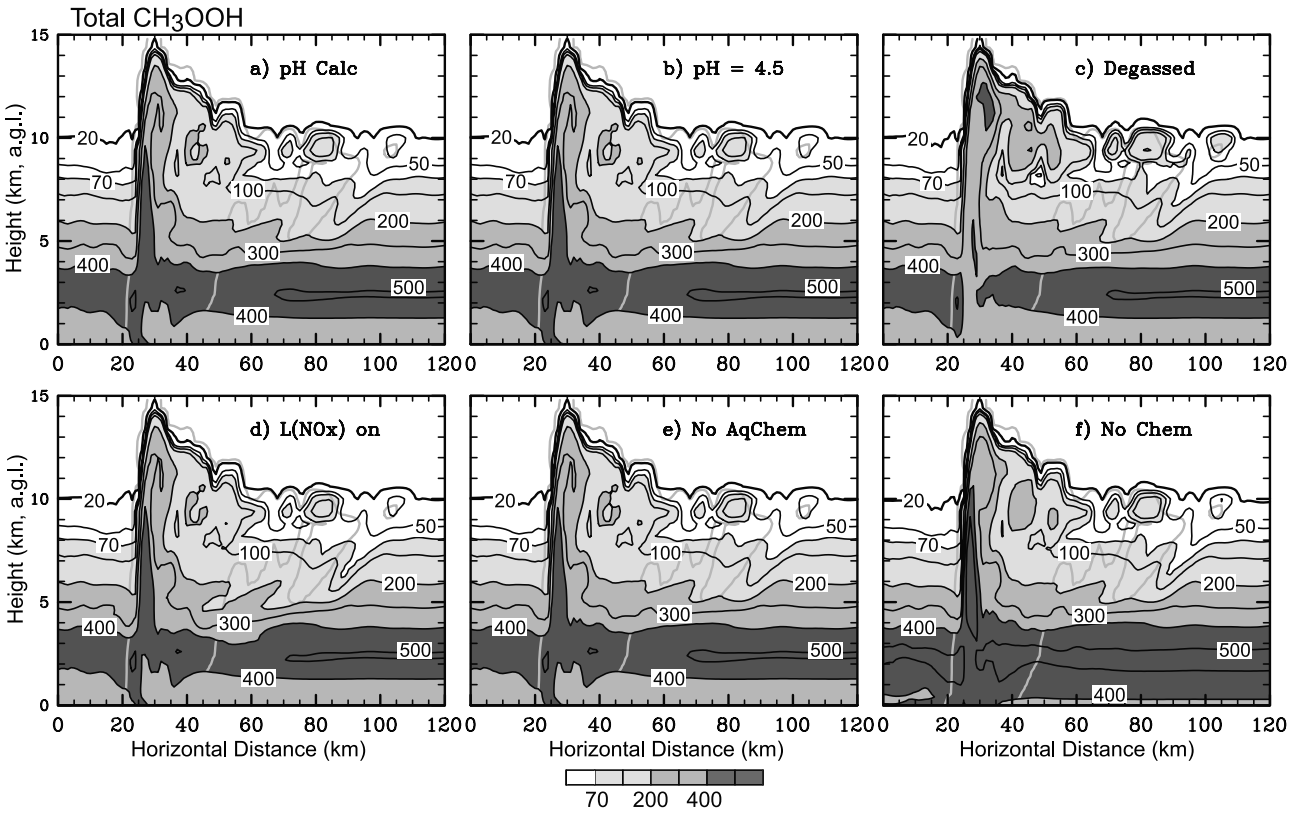

Figure 17. Total mixing ratios of CH_3OOH along the C-D cross section of Figure 15 at t = 5400 s for (a) the simulation where pH is calculated, (b) the simulation where pH is prescribed to 4.5, (c) the simulation where soluble species are degassed during drop freezing, (d) the simulation which includes NO_x production by lightning, (e) the simulation where aqueous chemistry does not occur, and (f) the simulation with no gas or aqueous chemistry. Contours are 20, 50, 70, 100, 200, 300, 400, and 500 pptv. The gray line is the total condensate mixing ratio equal to 0.01 g kg^{-1}.

differently from the ones presented here. The chemistry in the work of *DeCaria et al.* [2005] is calculated separately from the meteorology such that effects of microphysical processes are not represented. They assume that soluble species are either in the gas phase or in the liquid cloud droplets or rain but not in the frozen hydrometeors. Further comparisons of our simulations with the CSCTM-GCE model [*DeCaria et al.*, 2005] are described by *Barth et al.* 2007. Measured retention factors for volatile species vary significantly between the bounding values (0 and 1) used here [e.g., *Lamb and Blumenstein*, 1987; *Iribarne and Pyshnov*, 1990; *Snider et al.*, 1992; *Voisin et al.*, 2000]. Previous work to understand the retention factor [*Stuart and Jacobson*, 2003, 2004, 2006] indicates that it is likely highly dependent on the Henry's law constant, with higher solubility leading to greater retention. Retention factor values for intermediate solubility species, such as CH_2O and H_2O_2, are also predicted to depend on the freezing conditions (pH, temperature, drop size, drop speed) and therefore on the dominant ice microphysical processes occurring in the storm. Hence the retention factor is not likely constant in space or time in a given storm or between storms. Nonetheless, an intermediate value (for example, 0.5) is likely more representative than the bounding values used here. A retention factor of 0.5 may result in small increases in UT H_2O_2 as reported by *Cohan et al.* [1999]. In addition to improving the accuracy of the retention repre-

Table 7. Scavenging Efficiencies of the Soluble Tracers

Species	pH-Calc	pH = 4.5	Degassed	L(NOx)-On	No-AqChem	No-Chem
Water	26.9	26.9	26.9	26.9	26.9	26.9
CH_2O	45.7	57.1	11.1	45.8	64.1	66.5
CH_2O + HCOOH	59.8	64.2	14.9	59.9	64.1	66.5
H_2O_2	57.6	55.0	14.7	57.5	64.9	63.7
CH_3OOH	7.25	7.26	1.28	7.25	7.24	6.81
HNO_3	96.0	96.1	29.3	96.0	96.1	94.6
NH_3	88.8	88.8	31.9	88.8	88.8	88.8
SO_2 + SO_4^{2-}	58.8	55.4	16.9	58.8	47.0	46.4

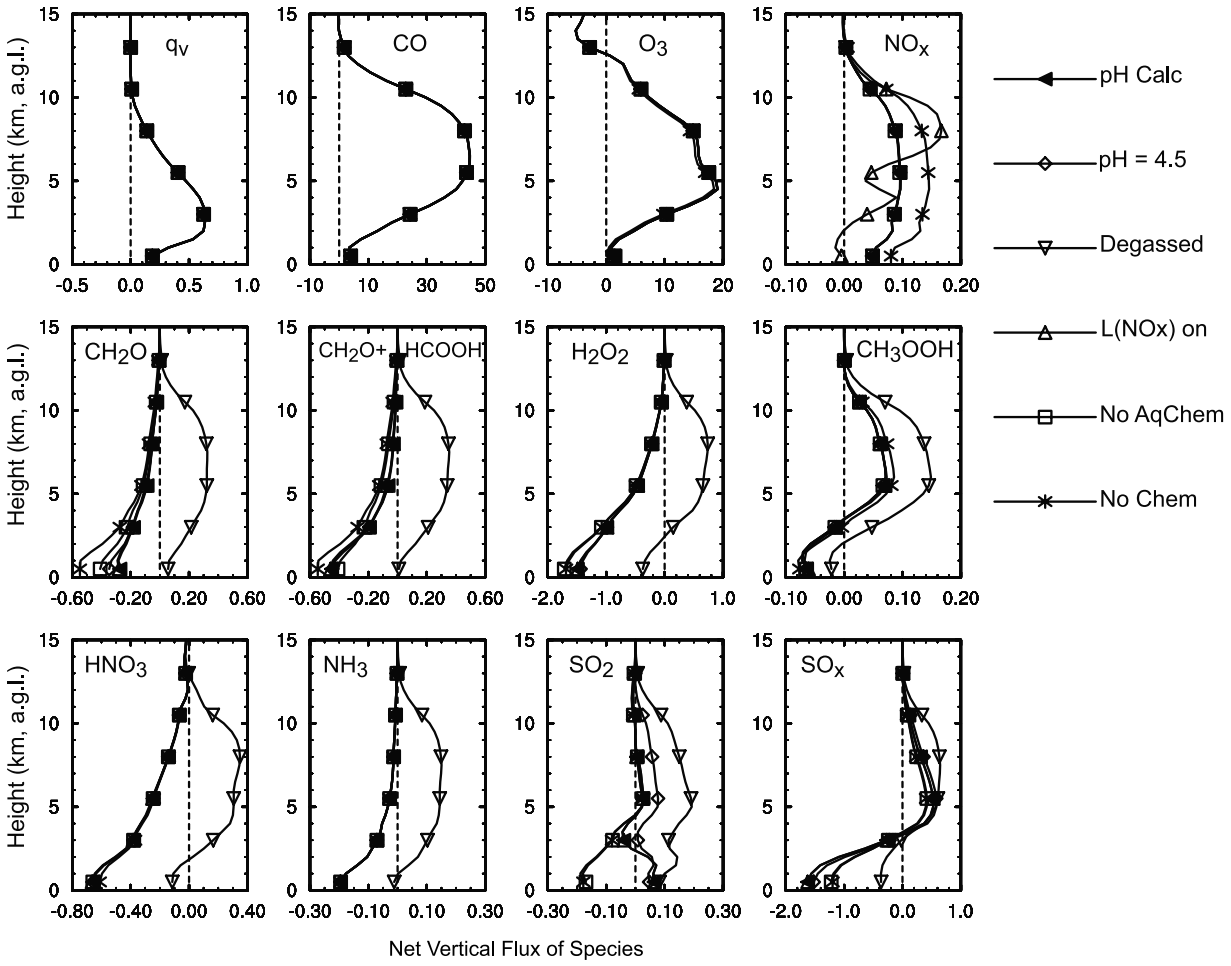

Figure 18. Net vertical fluxes which is a combination of the advection flux and precipitation flux for key chemical species as a function of altitude. Units for the water vapor flux is 10^{-2} kg m^{-2} s^{-1}. Units for the constituent fluxes are 10^{-9} mol m^{-2} s^{-1}.

sentation in modeling, field measurements are needed to help reduce this uncertainty.

[54] By comparing mixing ratios of CH_2O, H_2O_2, and CH_3OOH in the convective outflow region, the source strength of each of these species for HO_x radicals can be estimated. Although H_2O_2 undergoes significant scavenging by the storm, its mixing ratios (60–200 pptv) in the convective outflow are similar to the CH_3OOH mixing ratios (100–200 pptv, Figures 6 and 14). CH_2O mixing ratios (<50 pptv, Figures 6 and 7) in the convective outflow are smaller than either H_2O_2 or CH_3OOH. Hence H_2O_2 and CH_3OOH provide a similar source strength for HO_x radicals while CH_2O provides a smaller contribution to the HO_x source strength as it is injected into the UT. These results are based on chemistry that does not include nonmethane hydrocarbons, which could enhance CH_2O mixing ratios in the convective outflow. Nevertheless, these results support the hypotheses put forward by *Chatfield and Crutzen* [1984], *Prather and Jacob* [1997], and *Jaeglé et al.* [1997].

[55] Our simulations showed that the impact of NO_x produced by lightning was small for CH_2O, H_2O_2, and CH_3OOH in the flux analysis of wet deposition and fluxes into the UT region. We expect that this is a result of the analysis being near the lightning NO_x source during the storms' lifetime and that these species would be more impacted further downwind of the convection, in the same manner that O_3 is modified further downwind of convection [*Pickering et al.*, 1992b]. *Wang and Prinn* [2000] found significantly more CH_2O produced from their simulation that included a lightning NO_x source than that without lightning NO_x production. Their simulations were integrated for 30 hours which allowed time for the chemistry to proceed, while our short integration time of 3 hours does not allow for downwind chemistry to occur.

6. Conclusions

[56] A simple gas-aqueous chemistry scheme has been coupled to the Weather Research and Forecasting (WRF) model to examine the chemical redistribution of formaldehyde, formic acid, and peroxides by deep convection. The simulations were configured for idealized convection, that is, warm bubbles initiate the convection, and for O_3-NO_x-CH_4 chemistry. The radar reflectivity from the model results reasonably represents the observed CSU CHILL radar reflectivity for the 10 July 1996, STERAO-Deep Convection storm, suggesting that the simulation of cloud dynamics and structure (i.e., hydrometeor distribution) are realistic.

[57] The redistribution of formaldehyde, hydrogen peroxide, methyl hydrogen peroxide, and formic acid is examined

with several sensitivity simulations. Significantly different redistributions of these soluble species, including methyl hydrogen peroxide which has the lowest solubility of the four species studied, are found between two of the simulations: (1) the control simulation where the dissolved species is completely retained in the frozen cloud particle when cloud and raindrops freeze and (2) the sensitivity simulation where the dissolved species is completely degassed from the freezing drops. When a dissolved species is degassed, the species is primarily transported to the upper troposphere. Because the 10 July 1996 STERAO storm did not include concurrent measurements of any of these four species in both the inflow and outflow regions of deep convection, we cannot determine if one simulation more closely resembles observations than the others. Since the results from these two model runs are significantly different, it is important to measure these HO_x precursors in both convective inflow and outflow in order to understand better the influence of convection on upper troposphere ozone mixing ratios.

[58] Analysis of the anvil region found that CH_2O, H_2O_2, and CH_3OOH were primarily in the gas phase (85–95%) and only 5–15% of the species resided in the snow for the simulations in which it was assumed that dissolved gases are retained in freezing drops. The adsorption of gas-phase species onto the ice was not included in these simulations, and this process may alter the partitioning of these species between gas and snow.

[59] Comparisons of mixing ratios of CH_2O, H_2O_2, and CH_3OOH in the convective outflow indicate whether the species has a potential to produce HO_x radicals and subsequently O_3 in the upper troposphere. Our results show similar mixing ratios among the peroxides but smaller mixing ratios for CH_2O for the relatively clean chemical scenario and chemistry that did not include nonmethane hydrocarbons. The production of NO_x from lightning had little effect on these results.

[60] Mixing ratios of formic acid in the convective outflow were small (<20 pptv). Thus HCOOH may not be produced in sufficient quantity to be a reliable indicator of cloud-processed air. However, HCOOH mixing ratios will vary significantly with characteristics of the storm (larger liquid water regions will allow for more aqueous phase production of HCOOH) and with the pH of the cloud and rainwater.

[61] These model simulations highlight the uncertainties in predicting the influence of deep convection on upper tropospheric composition and chemistry for a single thunderstorm. The modeled thunderstorm is representative of a characteristic high plains storm with high cloud base, relatively larger regions of ice particles compared to liquid particles, and a sheared environment conducive to longer-lived storms. The convective transport and wet deposition of the HO_x precursors, CH_2O and H_2O_2, will vary among deep convective storms depending on the storm structure and dynamics. It is recommended that a variety of storms are sampled to understand better the convective influence on upper tropospheric composition.

[62] **Acknowledgments.** The National Center for Atmospheric Research is operated by the University Corporation for Atmospheric Research under the sponsorship of the National Science Foundation. K. Pickering and L. Ott acknowledge the support of NSF grant ATM-9912336 and NASA grant NAG5-11276. Comments and discussions with Alan Fried, Danny McKenna, and Brian Ridley are greatly appreciated as well as the assistance from Kaylee Acuff. Further information concerning the meteorological model can be found at http://wrf-model.org.

References

Barth, M. C., A. L. Stuart, and W. C. Skamarock (2001), Numerical simulations of the July 10, 1996 Stratospheric-Tropospheric Experiment: Radiation, Aerosols, and Ozone/Deep Convection Experiment storm: Redistribution of soluble tracers, *J. Geophys. Res.*, *106*, 12,381–12,400.

Barth, M. C., S. Sillman, R. Hudman, M. Z. Jacobson, C.-H. Kim, A. Monod, and J. Liang (2003), Summary of the cloud chemistry modeling intercomparison: Photochemical box model simulation, *J. Geophys. Res.*, *108*(D7), 4214, doi:10.1029/2002JD002673.

Barth, M. C., et al. (2007), Cloud-scale model intercomparison of chemical constituent transport in deep convection, *Atmos. Chem. Phys. Disc.*, *7*, 8035–8085.

Brasseur, G. P., D. A. Hauglustaine, S. Walters, P. J. Rasch, J.-F. Muller, C. Granier, and X. X. Tie (1998), MOZART, a global chemical transport model for ozone and related chemical tracers: Part 1. Model description, *J. Geophys. Res.*, *103*, 28,265–28,289.

Chameides, W. L. (1984), The photochemistry of a remote marine stratiform cloud, *J. Geophys. Res.*, *89*, 4739–4755.

Chatfield, R. B., and P. J. Crutzen (1984), Sulfur dioxide in remote oceanic air: Cloud transport of reactive precursors, *J. Geophys. Res.*, *89*, 7111–7132.

Cohan, D. S., M. G. Schultz, D. J. Jacob, B. G. Heikes, and D. R. Blake (1999), Convective injection and photochemical decay of peroxides in the tropical upper troposphere: Methyl iodide as a tracer of marine convection, *J. Geophys. Res.*, *104*, 5717–5724.

DeCaria, A. J., K. E. Pickering, G. L. Stenchikov, and L. E. Ott (2005), Lightning-generated NO_X and its impact on tropospheric ozone production: A three-dimensional modeling study of a Stratosphere-Troposphere Experiment: Radiation, Aerosols and Ozone (STERAO-A) thunderstorm, *J. Geophys. Res.*, *110*, D14303, doi:10.1029/2004JD005556.

Dickerson, R. R., et al. (1987), Thunderstorms: An important mechanism in the transport of air pollutants, *Science*, *235*, 460–465.

Dye, J. E., et al. (2000), An overview of the Stratospheric-Tropospheric Experiment: Radiation, Aerosols, and Ozone (STERAO)-Deep Convection experiment with results for the July 10, 1996 storm, *J. Geophys. Res.*, *105*, 10,023–10,045.

Easter, R. C., and J. M. Hales (1983), Interpretations of the OSCAR data for reactive gas scavenging, in *Precipitation Scavenging, Dry Deposition, and Resuspension*, edited by H. R. Pruppacher, R. G. Semonin, and W. G. N. Slinn, pp. 649–662, Elsevier, New York.

Fehr, T., H. Holler, and H. Huntrieser (2004), Model study on production and transport of lightning-produced NOx in a EULINOX supercell storm, *J. Geophys. Res.*, *109*, D09102, doi:10.1029/2003JD003935.

Flossmann, A. I., and W. Wobrock (1996), Venting of gases by convective clouds, *J. Geophys. Res.*, *101*, 18,639–18,649.

Giorgi, F., and W. L. Chameides (1986), Rainout lifetimes of highly soluble aerosols and gases as inferred from simulations with a general circulation model, *J. Geophys. Res.*, *91*, 14,367–14,376.

Hauf, T., P. Schulte, R. Alheit, and H. Schlager (1995), Rapid vertical trace gas transport by an isolated midlatitude thunderstorm, *J. Geophys. Res.*, *100*, 22,957–22,970.

Heikes, B. G., et al. (1996), Hydrogen peroxide and methylhydroperoxide distributions related to ozone and odd hydrogen over the North Pacific in the fall of 1991, *J. Geophys. Res.*, *101*, 1891–1905.

Helas, G., H. Bingemer, and M. O. Andreae (1992), Organic acids over equatorial Africa: Results from DECAFE 88, *J. Geophys. Res.*, *97*, 6187–6193.

Hoffmann, M. R., and J. G. Calvert (1985), Chemical transportation modules for Eulerian acid deposition models, vol. II, The aqueous-phase chemistry, *Rep. EPA/600/3-85/017*, Environ. Prot. Agency, Research Triangle Park, N. C.

Iribarne, J. V., and T. Pyshnov (1990), The effect of freezing on the composition of supercooled droplets: I. Retention of HCl, HNO_3, NH_3, and H_2O_2, *Atmos. Environ., Part A*, *24A*, 383–387.

Jaeglé, L., et al. (1997), Observed OH and HO_2 in the upper troposphere suggest a major source from convective injection of peroxides, *Geophys. Res. Lett.*, *24*, 3181–3184.

Jaeglé, L., D. J. Jacob, W. H. Brune, and P. O. Wennberg (2001), Chemistry of HO_x radicals in the upper troposphere, *Atmos. Environ.*, *35*, 469–489.

Kim, C.-H., S. M. Kreidenweis, G. Feingold, G. J. Frost, and M. K. Trainer (2002), Modeling cloud effects on hydrogen peroxide and methylhydroperoxide in the marine atmosphere, *J. Geophys. Res.*, *107*(D2), 4018, doi:10.1029/2000JD000285.

Lamb, D., and R. Blumenstein (1987), Measurement of the entrapment of sulfur dioxide by rime ice, *Atmos. Environ.*, *21*, 1765–1772.

Lelieveld, J., and P. J. Crutzen (1991), The role of clouds in tropospheric photochemistry, *J. Atmos. Chem.*, *12*, 229–267.

Li, S.-M., K. G. Anlauf, H. A. Wiebe, and J. W. Bottenheim (1994), Estimating primary and secondary production of HCHO in eastern North America based on gas phase measurements and principal component analysis, *Geophys. Res. Lett.*, *21*, 669–672.

Lin, Y.-L., R. D. Farley, and H. D. Orville (1983), Bulk parameterization of the snow field in a cloud model, *J. Clim. Appl. Meteorol.*, *22*, 1065–1092.

Liu, S. C., M. Trainer, F. C. Fehsenfeld, D. D. Parrish, E. J. Williams, D. W. Fahey, G. Huebler, and P. C. Murphy (1987), Ozone production in the rural troposphere and the implications for regional and global ozone distributions, *J. Geophys. Res.*, *92*, 4191–4207.

Madronich, S., and S. Flocke (1999), The role of solar radiation in atmospheric chemistry, in *Handbook of Environmental Chemistry*, edited by P. Boule, pp. 1–26, Springer, New York.

Mari, C., D. J. Jacob, and P. Bechtold (2000), Transport and scavenging of soluble gases in a deep convective cloud, *J. Geophys. Res.*, *105*, 22,255–22,267.

Ott, L. E., K. E. Pickering, G. L. Stenchikov, H. Huntrieser, and U. Schumann (2007), Effects of lightning NOx production during the 21 July European Lightning Nitrogen Oxides Project storm studied with a three-dimensional cloud-scale chemical transport model, *J. Geophys. Res.*, *112*, D05307, doi:10.1029/2006JD007365.

Pickering, K. E., A. M. Thompson, R. R. Dickerson, W. T. Luke, D. P. McNamara, J. Greenberg, and P. R. Zimmerman (1990), Model calculations of tropospheric ozone production potential following observed convective events, *J. Geophys. Res.*, *95*, 14,049–14,062.

Pickering, K. E., J. R. Scala, A. M. Thompson, W.-K. Tao, and J. Simpson (1992a), A regional estimate of convective transport of CO from biomass burning, *Geophys. Res. Lett.*, *19*, 289–292.

Pickering, K. E., A. M. Thompson, J. R. Scala, W.-K. Tao, R. R. Dickerson, and J. Simpson (1992b), Free tropospheric ozone production following entrainment of urban plumes into deep convection, *J. Geophys. Res.*, *97*, 17,985–18,000.

Pickering, K. E., et al. (1996), Convective transport of biomass burning emissions over Brazil during TRACE A, *J. Geophys. Res.*, *101*, 23,993–24,012.

Prather, M. J., and D. J. Jacob (1997), A persistent imbalance in HO_x and NO_x photochemistry of the upper troposphere driven by deep tropical convection, *Geophys. Res. Lett.*, *24*, 3189–3192.

Price, C., J. Penner, and M. Prather (1997), NOx from lightning: 1. Global distribution based on lightning physics, *J. Geophys. Res.*, *102*, 5929–5941.

Ridley, B. A., J. E. Dye, J. G. Walega, J. Zheng, F. E. Grahek, and W. Rison (1996), On the production of active nitrogen by thunderstorms over New Mexico, *J. Geophys. Res.*, *101*, 20,985–21,005.

Sander, R. (1999), Compilation of Henry's law constants for inorganic and organic species of potential importance in environmental chemistry (version 3), *Tech. rep.*, Max Planck Inst.-Chemie, http://www.mpch-mainz. mpg.de/sander/res/henry.html.

Sander, S. P., et al. (2003) Chemical kinetics and photochemical data for use in atmospheric studies, evaluation no. 14, Tech. rep., Jet Propulsion Laboratory, California Institute of Technology, JPL Publ. 02-25, http://jpldataeval.jpl.nasa.gov.

Sanhueza, E., M. Santana, D. Trapp, C. deServes, L. Figueroa, R. Romero, A. Rondon, and L. Donoso (1996), Field measurement evidence for an atmospheric chemical source of formic and acetic acids in the tropic, *Geophys. Res. Lett.*, *23*, 1045–1048.

Scala, J. R., et al. (1990), Cloud draft structure and trace gas transport, *J. Geophys. Res.*, *95*, 17,015–17,030.

Schwartz, S. E. (1986), Mass-transport considerations pertinent to aqueous phase reactions of gases in liquid-water clouds, in *Chemistry of Multiphase Atmospheric Systems*, edited by W. Jaeschke, pp. 415–471, Springer, New York.

Seifert, A., and M. Weisman (2005), A comparison of bulk microphysical schemes for cloud resolving NWP, in *6th WRF / 15th MM5 Users' Workshop*, pp. http://www.mmm.ucar.edu/wrf/users/workshops/WS2005/abstracts/Session6/2-Seifert.pdf, Boulder, Colorado.

Skamarock, W. C., et al. (2000), Numerical simulations of the July 10 Stratospheric-Tropospheric Experiment: Radiation, Aerosols, and Ozone/Deep Convection Experiment convective system: Kinematics and transport, *J. Geophys. Res.*, *105*, 19,973–19,990.

Skamarock, W. C., J. E. Dye, E. Defer, M. C. Barth, J. L. Stith, B. A. Ridley, and K. Baumann (2003), Observational-and modeling-based budget of lightning-produced NO_x in a continental thunderstorm, *J. Geophys. Res.*, *108*(D10), 4305, doi:10.1029/2002JD002163.

Skamarock, W. C., J. B. Klemp, J. Dudhia, D. Gill, D. Barker, W. Wang, and J. G. Powers (2005), A description of the Advanced Research WRF Version 2., *Technical note NCAR/TN-468+STR*, NCAR, Boulder, CO.

Snider, J. R., D. C. Montague, and G. Vali (1992), Hydrogen peroxide retention in rime ice, *J. Geophys. Res.*, *97*, 7569–7578.

Stuart, A. L., and M. Z. Jacobson (2003), A timescale investigation of volatile chemical retention during hydrometeor freezing: Nonrime freezing and dry growth riming without spreading, *J. Geophys. Res.*, *108*(D6), 4178, doi:10.1029/2001JD001408.

Stuart, A. L., and M. Z. Jacobson (2004), Chemical retention during dry growth riming, *J. Geophys. Res.*, *109*, D07305, doi:10.1029/2003JD004197.

Stuart, A. L., and M. Z. Jacobson (2006), A numerical model of the partitioning of trace chemical solutes during drop freezing, *J. Atmos. Chem.*, *53*, 13–42.

Tremblay, A. (1987), Cumulus cloud transport, scavenging, and chemistry: Observations and simulations, *Atmos. Environ.*, *21*, 2345–2364.

Voisin, D., D. C. Montague, and G. Vali (2000), Scavenging of acidic gases (HCOOH, CH_3COOH, HNO_3, HCl, and SO_2) and ammonia in mixed liquid-solid water clouds at the Puy de Dome mountain (France), *J. Geophys. Res.*, *105*, 6817–6836, doi:10.1029/1999JD900983.

Wang, C. (2005), A modeling study of the response of tropical deep convection to the increase of cloud condensation nuclei concentration: 2. Radiation and tropospheric chemistry, *J. Geophys. Res.*, *110*, D22204, doi:10.1029/2005JD005829.

Wang, C., and P. J. Crutzen (1995), Impact of a simulated severe local storm on the redistribution of sulfur dioxide, *J. Geophys. Res.*, *100*, 11,357–11,367.

Wang, C., and R. G. Prinn (2000), On the roles of deep convective clouds in tropospheric chemistry, *J. Geophys. Res.*, *105*, 22,269–22,290.

Wennberg, P. O., et al. (1998), Hydrogen radicals, nitrogen radicals, and the production of O_3 in the upper troposphere, *Science*, *279*, 49–53.

Wicker, L. J., and W. C. Skamarock (2002), Time splitting methods for elastic models using forward time schemes, *Mon. Weather Rev.*, *130*, 2088–2097.

Winkler, A. K., N. S. Holmes, and J. N. Crowley (2002), Interaction of methanol, acetone and formaldehyde with ice surfaces between 198 and 223 K, *Phys. Chem. Chem. Phys.*, *4*, 5270–5275.

Yin, Y., K. S. Carslaw, and D. J. Parker (2002), Redistribution of trace gases by convective clouds-mixed phase processes, *Atmos. Chem. Phys.*, *2*, 293–306.

M. C. Barth and W. C. Skamarock, National Center for Atmospheric Research, Boulder, CO, USA. (barthm@ncar.ucar.edu)

S.-W. Kim, NOAA/Earth System Research Laboratory, CSDO4 325 Broadway, Boulder, CO 80305, USA.

L. E. Ott and K. E. Pickering, Department of Atmospheric and Oceanic Science, University of Maryland, College Park, MD, USA.

A. L. Stuart, Department of Environmental and Occupational Health, University of South Florida, Tampa, FL, USA.